MIT Libraries | DSpace@MIT

MIT Open Access Articles

Studying the effects of elongational properties on atomization of weakly viscoelastic solutions using Rayleigh Ohnesorge Jetting Extensional Rheometry (ROJER)

Massachusetts Institute of Technology

Title: Studying the Effects of Elongational Properties on Atomization of Weakly Viscoelastic Solutions Using Rayleigh Ohnesorge Jetting Extensional Rheometry (ROJER)

Corresponding Author: Mr. Bavand Keshavarz, PhD candidate

Corresponding Author's Institution: Department of Mechanical Engineering, Massachussetts Institute of Technology, Cambridge, MA. 02139

First Author: Bavand Keshavarz, PhD candidate

Order of Authors: Bavand Keshavarz, PhD candidate; Vivek Sharma, Professor; Eric C Houze; Michael R Koerner; John R Moore; Patricia M Cotts; Philip Threlfall-Holmes; Gareth H McKinley, Professor

Abstract: The extensional rheological properties of dilute polymer solutions play a dominant role in many commercial processes such as air-assisted atomization. This is a high deformation rate process important in application of diverse materials such as paints, fertilizer sprays and delivery of airborne drugs. Dilute polymeric solutions which have identical values of high shear-rate viscosity (HSV) often exhibit different values of Sauter Mean Diameter (SMD) in their spray size distributions as a result of differing extensional rheological properties. We explore the atomization of a series of model Poly(ethylene oxide) (PEO) solutions dissolved in water/glycerol mixtures. Each solution is sprayed with an air-assisted spray gun under similar conditions and imaged with a commercial spray measurement system. The values of HSV for PEO solutions are close to the solvent viscosity and matched to those of typical ink or paint samples. The surface tensions of the fluids are also tuned to be very similar, however both the SMD and the droplet size distribution change considerably. For the highest molecular weight PEO systems, interconnected beads-on-string structures are observed at different positions of the spray fan. Capillary Break-up Extensional Rheometry (CaBER) can be used to measure the extensional properties of the more viscous solutions, but the well-known limitations of this approach include inertially-induced asymmetries, gravitational sagging and the very short filament lifetimes of low viscosity samples all of which constrain the range of relaxation times that can be probed. Consequently we also explore the use of Rayleigh Ohnesorge Jet Elongational Rheometry (ROJER) to probe the extensional response of these viscoelastic solutions at realistic timescales and deformation rates. A cylindrical liquid jet is excited by a piezo-actuator at a known frequency as it exits a micromachined nozzle, and stroboscopic imaging provides high temporal and spatial resolution in the break-up process. Analyzing the evolution in the jet diameter before break-up enables meaningful measurement of relaxation times down to values as small as 60 microsecond, and these values can be directly correlated with the differences in the final spray size distributions and the mean diameters. We outline a simple model for the fluid dynamics of the thinning filaments close to breakup that accurately describes the variation of the average droplet diameter as a function of the elongational relaxation time measured for each fluid.

Studying the Effects of Elongational Properties on Atomization of Weakly Viscoelastic Solutions Using Rayleigh Ohnesorge Jetting Extensional Rheometry (ROJER)

Bavand Keshavarz[*1], Vivek Sharma[†2], Eric C. Houze[‡3], Michael R. Koerner[§3], John R. Moore[¶3], Patricia M. Cotts[∥4], Philip Threlfall-Holmes[**5], and Gareth H. McKinley[††1]

[1]Department of Mechanical Engineering, Massachussetts Institute of Technology, Cambridge, MA. 02139

[2]Department of Chemical Engineering, University of Illinois at Chicago

[3]Axalta Coating Systems, Experimental Station E402/2239, Wilmington, DE. 19803

[4]DuPont CR&D, Experimental Station, Wilmington, DE. 19803

[5]AkzoNobel Supply Chain, Research and Development, Stoneygate Lane, Felling, Gateshead, NE10 0JY, UK

July 10, 2014

Abstract

The extensional rheological properties of dilute polymer solutions play a dominant role in many commercial processes such as air-assisted atomization. This is a high deformation

[*]bavand@mit.edu

[†]viveks@uic.edu

[‡]eric.c.houze@axaltacs.com

[§]michael.r.koerner@axaltacs.com

[¶]john.r.moore@axaltacs.com

[∥]Patricia.M.Cotts-1@dupont.com

[**]Philip.Threlfall-Holmes@akzonobel.com

[††]gareth@mit.edu

rate process important in application of diverse materials such as paints, fertilizer sprays and delivery of airborne drugs. Dilute polymeric solutions which have identical values of high shear-rate viscosity (HSV) often exhibit different values of Sauter Mean Diameter (SMD) in their spray size distributions as a result of differing extensional rheological properties. We explore the atomization of a series of model Poly(ethylene oxide) (PEO) solutions dissolved in water/glycerol mixtures. Each solution is sprayed with an air-assisted spray gun under similar conditions and imaged with a commercial spray measurement system. The values of HSV for PEO solutions are close to the solvent viscosity and matched to those of typical ink or paint samples. The surface tensions of the fluids are also tuned to be very similar, however both the SMD and the droplet size distribution change considerably. For the highest molecular weight PEO systems, interconnected beads-on-string structures are observed at different positions of the spray fan. Capillary Break-up Extensional Rheometry (CaBER) can be used to measure the extensional properties of the more viscous solutions, but the well-known limitations of this approach include inertially-induced asymmetries, gravitational sagging and the very short filament lifetimes of low viscosity samples all of which constrain the range of relaxation times that can be probed. Consequently we also explore the use of Rayleigh Ohnesorge Jet Elongational Rheometry (ROJER) to probe the extensional response of these viscoelastic solutions at realistic timescales and deformation rates. A cylindrical liquid jet is excited by a piezo-actuator at a known frequency as it exits a micromachined nozzle, and stroboscopic imaging provides high temporal and spatial resolution in the break-up process. Analyzing the evolution in the jet diameter before break-up enables meaningful measurement of relaxation times down to values as small as $60 \ \mu s$, and these values can be directly correlated with the differences in the final spray size distributions and the mean diameters. We outline a simple model for the fluid dynamics of the thinning filaments close to breakup that accurately describes the variation of the average droplet diameter as a function of the elongational relaxation time measured for each fluid.

1   Introduction

Jet atomization and the physics of liquid breakup has been a source of scientific curiosity and industrial applications for many years and over the past century there have been many developments in understanding the fluid mechanics involved in jetting and atomization of the Newto-

nian liquids [1]. However most liquids of commercial relevance have a complex microstructure and do not completely follow Newtonian behavior; polymer melts, fuels, paints, and our own saliva are just a few examples. There are many applications in which these non-Newtonian solutions experience jet breakup or atomization such as paint spraying, inkjet printing, cosmetics preparation, spray drying of foods, and disease transfer through sneezing; however by comparison to the depth of knowledge about the atomization of Newtonian liquids [2, 3] little is known about the complexities encountered in the atomization of viscoelastic liquids [4]. Accurately measuring the extensional response of low viscosity fluids and understanding the importance of extensional stresses in complex flow fields is a research challenge that Ken Walters and colleagues focused on intensely for several decades. In a wide-ranging plenary paper for the 11th ICR in Brussels (1992) [5], Walters pointed out when discussing the challenges inherent to measuring the extensional properties of mobile liquids that "the task is therefore to generate a flow which is dominated by extension and to address the problem of how best to interpret the data in terms of material functions that are rheologically meaningful". He went on to note that (after he first expanded on this philosophy at an earlier 1984 European Congress) "...to say that it did not meet with unbridled enthusiasm would be an under-statement!" However, inspired by this conviction, and undeterred by such reservations we investigate air-blast atomization of complex fluids by seeking to understand and quantify the break up dynamics of a non-Newtonian jet.

Previous studies have shown that addition of viscoelasticity can lead to significant changes in both jet break up and atomization processes [6–9]. These modifications occur mainly when the fluid element reaches the large strains and rapid nonlinear deformation rates that are generated in the final breakup and pinch off stages (Figure 1). Chao et al.[7] showed that addition of polymers to jet fuels can lead to anti-misting properties which can be extremely beneficial to aviation safety. In some other applications such as spray or roll coating [10] these "anti-misting" properties which result from the added viscoelasticity may inhibit the sprayability of a liquid and be undesirable. Thus, understanding and quantifying these effects is an important scientific goal; better knowledge of these phenomena is sufficiently important that it has been suggested that the future of industries such as rapid manufacturing of biological materials via drop-on-demand printing or jet engine propulsion are dependent on new developments and

deeper understanding of jetting phenomena in complex fluids [11–14].

Attempts to understand the effects of viscoelasticity on atomization [4,15] have faced challenges in measuring the behavior of the non-Newtonian liquid in the strong nonlinear deformation and high strain rates that characterize the spray. Viscoelastic liquids are known to show nonlinear behavior in large deformations and demonstrate higher resistance against elongational deformations [16]. Spray visualizations show that the added viscoelasticity does not lead to any significant change in the early stages of breakup dynamics, when the liquid is still close to the nozzle. Here the deformations are still small and disturbances are in the linear stage (compare Figures 1(a) and 1(c)). However significant differences start to emerge when viscoelastic ligaments are stretched and elongated into the air stream far from the nozzle (compare Figures 1(b) and 1(d)). This has motivated many researchers to focus on the extensional rheological properties of the fluid, in order to better understand the effects of viscoelasticity on the liquid's performance in atomization [7, 17, 18]. These findings have shown qualitatively that the additional resistance against elongational deformations for viscoelastic solutions will lead to poor atomization. Precise measurements of elongational properties such as the fluid relaxation time or the magnitude of the elongational viscosity are essential for a quantitative study of these effects, but elongational rheology for dilute solutions is a well-known challenge [19–24]. While true extensional rheometers such as the Filament Stretching Extensional Rheometer (FISER) work well for very elastic melts, gels and viscous polymer solutions [25] there are only a few extensional rheometers that can be used for dilute polymer solutions and low viscosity complex fluids. James and Walters [20] provide a critical appraisal of many proposed techniques including the opposed jet rheometer and converging flow devices [26]; they argue that many of these instruments may be best thought of as rheological indexers rather than true rheometers. Although diverse industrial applications have benefited from these different rheological indexers, the need for an extensional rheometer for very dilute solutions persists. One well-known example is the Capillary Breakup Extensional Rheometer (CaBER) [27] which can work well for many dilute and semi-dilute polymeric solutions [24]. However Rodd et al.[21] have shown that even this capillary thinning technique has some limits in measurements and fails to generate a well-defined extensional flow-field if the relaxation time and viscosity of the liquid are both lower than certain limits. Extending the lower range of capabilities of filament thinning

devices through the use of novel strategies and designs is an active area of current research [28–31].

To understand the dominant effects of complex fluid rheology on atomization, researchers have tried to understand the key fluid mechanical features of sprays and study the dynamical response of well-characterized fluids in the spray. Recent research on air-assisted atomization has shown that, for a Newtonian fluid at least, this process can be described as a well characterized sequence of instabilities that help to finally disintegrate the liquid into small fragments (Figure 2). Marmottant and Villermaux [3] have shown that in air-assisted atomization the liquid jet passes through three distinct instabilities. Initially the low momentum core liquid jet experiences a relatively high shear rate at its surface induced by the surrounding annular flow of air (which has a much higher velocity and kinetic energy). This will lead to the generation of waves on the surface of the liquid jet due to the well-known Kelvin-Helmholtz instability (Figure 2) [32]. As the wave crests grow, the acceleration of the less dense medium, i.e. air, into the more dense medium results in a second instability, known as Rayleigh-Taylor instability, that elongates ligaments of fluid into the air stream. Finally the stretched ligaments thin down in the neck region that still connects them to the core liquid jet as a result of Rayleigh-Plateau instability and they ultimately detach from the jet after stretching to a certain length. Beyond this point the detached ligament can fragment into a cascade of small droplets which form the final spray mist.

For measurements of elongational properties in very low viscosity "mobile liquids", Christanti and Walker [18,33] used a novel method, originally suggested by Schümmer and Tebel [34] that focused on undertanding the fluid mechanics of the jet breakup process itself. By studying the jet breakup of dilute polymeric solutions they showed that there is a correlation between the measured relaxation times and the average droplet diameters measured in air-assisted atomization. Studies of sprays of viscoelastic solutions by Christanti and Walker [18], building on earlier work by Ferguson et al. [35], have shown qualitatively that there is an initial increase in average droplet diameters denoted by $< d >$ with increasing relaxation times followed by a saturation at higher values of the fluid relaxation time.

Despite the growing interest in fragmentation and atomization of very dilute polymeric solutions, there is still a lack of quantitative knowledge about the effects of viscoelasticity on

atomization in this limit. In this paper we outline a method for addressing the challenges in extensional rheology for very dilute solutions by studying a selection of dilute Poly(ethylene oxide) (PEO) solutions at moderate molecular weights and concentrations well below coil overlap conditions. We show that careful analysis of jet breakup for these liquids can help us make precise measurements of their elongational properties. The material property extracted from this forced jet rheometer is then compared with linear stability predictions for the hydrodynamics of this flow field and scalings from polymer physics for the relaxation times. These model solutions are also tested in a commercial air-assisted atomization gun, used in the paint coating industry, and the changes in the measured mean droplet size from the spray tests are related to the measured fluid relaxation times by a simple physical argument describing the fluid dynamics of the thinning and elongating ligaments that develop close to individual pinch off events in the spray.

2   Test Fluid Rheology

In order to systematically study the effects of viscoelasticity on the atomization, four different dilute polymer solutions were selected as test liquids. All of these solutions are made by dissolving small amounts of Poly(ethylene oxide) or (PEO) with $M_w = 3 \times 10^5 g/mol$ and $1 \times 10^6 g/mol$ respectively (purchased from Sigma Aldrich) in a water-glycerol (60-40 wt.%) solvent ($\eta_s = 3.2 mPa.s$) and the resulting viscometric properties are summarized in Table 1. The values of surface tension for all the viscoelastic solutions are close to the solvent value ($\sigma \simeq 60 \pm 3\, mN/m$). Using the expressions given in the [21, 36] the overlap concentrations (c^*) are respectively 0.28 wt.% and 0.14 wt.% for 300K and 1000K solutions. Values of the extensibility parameter for these PEO solutions are calculated based on the constants reported in [37] for flexible PEO chains ($L \sim M_w^{1-\nu}$ in which $\nu = 0.56$ for a reasonably good solvent such as PEO in water/glycerol). Because of the dissolved polymer, the shear viscosity of the solutions show a slight increase at low rates ($\eta_0 = 3.3 mPa.s$) and asymptotically approach the solvent value at high shear rates ($\eta_\infty = 3.2 mPa.s$ at $\dot{\gamma} \simeq 10^5\ s^{-1}$). The small increase in the zero shear viscosity is due to the very low concentration of the PEO in the solvent for this solution ($\eta_0 \simeq \eta_s (1 + c/c^*)$ and for the $M_w = 300K$ solution, $c/c^* = 0.036$). Although the

addition of small amounts of PEO to a Newtonian solvent will keep the shear viscosity almost unchanged, the extensional viscosity can increase substantially beyond a critical deformation rate [38]. This increase in the extensional viscosity arises from the coil-stretch transition of the dissolved macromolecules in a strong extensional flow [16]. One important measure for quantifying the onset of strain hardening is the elongational relaxation timescale (τ_E) of the fluid which varies with the molecular weight and concentration of dissolved polymer. The measured relaxation times for all the viscoelastic solutions determined through jet breakup studies are tabulated in Table 1. The details of these measurements will be discussed in more detail in sections 4 and 5.

3 Experimental Setup

The spray experiments were carried out using an air-assisted atomization nozzle (Figure 2(a)). The liquid jet is released at moderate speeds ($1 \leq V_{liquid} \leq 10 ms^{-1}$) through a cylindrical nozzle and this core flow is surrounded by a high speed annular flow of air ($V_{air} \sim 80 - 120\ ms^{-1}$). The destabilized liquid jet will then form a so-called "spray fan"; two auxiliary low speed jets of air are blown from the sides to keep the vertical axis of the spray fan as stable as possible. Visualization of the droplets after breakup are carried out using a LaVision imaging setup. A $1.5mm \times 1.5mm$ field of view is illuminated using laser back-lighting and digital images of the droplets were taken as they pass through the frame (Figure 4(b)). Image-processing and size distribution measurements of the droplets in the captured images were carried out by the LaVision image analysis package. Five different positions in the spray plane were selected as the sampling sites for all of the tested liquids and more than one thousand droplets were counted in each sampling. All the tests were performed for a fixed flow/geometry and similar environmental conditions in terms of temperature and humidity.

The viscometric properties of the fluids were measured using a stress-controlled rheometer (ARG2 with a $4mm$ cone geometry with $2°$ degree cone angle; TA Instruments), at low shear rates ($10s^{-1} \leq \dot{\gamma} \leq 1000s^{-1}$), and using a micro-fluidic rheometer (m-VROC from Rheosense) at higher shear rates ($1000s^{-1} \leq \dot{\gamma} \leq 200,000s^{-1}$). Extensional rheological properties are measured using capillary thinning rheometry and a free jet rheometer adopted from ideas first

discussed by Schümmer and Tebel [39]. Details of the CaBER technique have already been discussed in great detail in the literature [21,24,31]. To extend measurements to lower viscosity systems we use a jet breakup visualization apparatus shown schematically in Figure 4(a). A high pressure syringe pump (PHD ULTRA-4400 from Harvard Apparatus) pushes the test fluid through a $150\mu m$ diameter ceramic nozzle. Periodic perturbations are imposed on the fluid before entering the nozzle via an annular peizoelectric actuator. The imposed perturbations introduce very small sinusoidal modulations to the fluid jet with amplitudes less than 1% of the jet diameter over a user-selectable range of frequencies $(0.1Hz \leq f \leq 1 \times 10^5 Hz)$. If the wavenumber $k = 2\pi/\lambda$ (where λ is the wavelength) of the imposed perturbations lies in the unstable region of the Rayleigh-Plateau instability then the amplitude of these modulations will start to grow exponentially with time as the waves are convected downstream with the jet. Due to the periodic nature of the perturbation, the jet modulation is periodic and wave-like with crests and troughs appearing at a frequency identical to the drive frequency of the piezoelectic actuator. This enables us to use stroboscopic imaging to avoid the common challenges of imaging these rapid time-varying phenomena. High speed imaging of jet breakup requires capturing movies at high frame rates and high magnification, consequently the images often have low resolutions or poor illumination due to physical limitations of cameras at these high frame rates. The strobe imaging setup used in this study is adopted from an inkjet visualization device made by JetXpert. The strobed LED light can generate very short and bright light pulses (with less than $1\mu s$ exposure duration) over a wide range of frequencies $(0.1 - 1 \times 10^5 Hz)$. This allows us to tune the strobe frequency and set it very close to the drive frequency ($f_{strobe} = f_{piezo} - \Delta f$). Thus the captured movie slows down the real motion by a large factor (e.g. for $f_{piezo} = 6000Hz$ and a frequency shift of $\Delta f = 0.1Hz$ the resulting motion is slowed down by a factor of $\Delta f / f_{piezo} \sim 1/60,000$; see Appendix A for additional details). Using this approach we avoid the necessity of capturing movies at very high frame rates and with sufficient memory we can capture sharp and high resolution time-resolved images (1024×778 pixels) of the jet breakup process (see the movie in Supporting Information).

The apparent jet velocity in the captured movies (denoted by V_{app}) is calculated from the expression:

$$V_{app}[m/s] = MF.V_{dig}.FR \qquad (1)$$

where MF is the magnification factor of the optics in μm per pixel, V_{dig} is the digital velocity of the jet (in pixels traveled per frame), and FR is the frame rate of the captured movie (in frames per second). Although the relationship in Eq. (1) can be used to find the apparent velocity of a wave crest or droplet from the digital velocity, as a result of the strobe effect the apparent velocity is not the real velocity at which the fluid is convected. The real jet velocity can be directly calculated from the flow rate of the pump:

$$V_j = Q/\pi R_0^2 \tag{2}$$

where Q is the volumetric flow rate and R_0 is the radius of the nozzle. The real velocity and the apparent velocity are connected to each other by the strobe principle [40] (see Appendix A for derivation):

$$V_{app} = \frac{\Delta f}{f_{piezo}} V_j \tag{3}$$

where, as mentioned before, f_{piezo} is the drive frequency and $f_{piezo} - \Delta f$ is the strobe frequency. Similarly to calculate the real elapsed time over which the fluid particle has been moving away from the nozzle we only need to know the axial distance traveled (Z) and from that the time of flight can be calculated:

$$t = Z/V_j \tag{4}$$

where Z is the axial position and is equal to $Z_0 + \Delta Z$ in which Z_0 is the location of the top line of the image frame and ΔZ is the relative distance measured from this reference point. This can be measured by precise position tracking of the stepper motor which moves the nozzle that is mounted on a one axis translation stage (see Figure 4(a)). Although Eqs. (1) and (3) show how the real and apparent velocities are connected, it is more convenient (and also less prone to error propagation) to calculate the time of flight for a fluid element exiting the nozzle by simply using Eqs. (2) and (4). Given a specified flow rate (controlled by the syringe pump) the real velocity of the jet can be measured and the actual elapsed time of flight is calculated by Eq. (4).

For the instability of interest, i.e. Rayleigh-Plateau instability, the perturbations will be convected downstream with the jet velocity and our assumptions for using Eq. (4) are correct.

This is a result of the fact that instability is convective in nature and theoretical analysis shows that (over the range of tested Weber numbers) there are no absolute instabilities, in which perturbations increase in amplitude at all positions in the jet (see [41] for additional details). Thus the imposed perturbation at a given frequency f_{piezo} will make waves with wavelength $\lambda = V_j/f_{piezo}$ which are convected away from the nozzle with the jet velocity V_j. This means that the dimensionless wavenumber of the imposed disturbance is equal to:

$$kR_0 = 2\pi f_{piezo}R_0/V_j \qquad (5)$$

in order to see these waves grow rather than decay with time it is crucial to keep the range of the disturbance in the instability margin which lies between $0 \leq kR_0 \leq 1$ [32].

Once the movies have been recorded the captured images are analyzed using image processing codes written in MATLAB and the evolution of the liquid filament diameter with time can be calculated using an edge detection algorithm.

4 Capillary Breakup Extensional Rheometry (CaBER)

From the early days of extensional rheometry [42] accurate measurement of elongational properties for a wide range of materials/liquids has been reported as an experimental challenge [19, 22, 23] due to the fact that there are few possible geometries/conditions in which uniaxial extensional flows dominate and shear effects are negligible. Although some known established devices such as FISER (Filament Stretching Extensional Rheometer[43]) or SER (Sentmanat Extensional Rheometer[44, 45]) have shown very promising results for sufficiently viscoelastic polymer melts and solutions, there are still many additional challenges for measuring the extensional rheology of very dilute solutions.

Bazilevsky et al. [46] showed that understanding the viscoelastic fluid dynamics of polymeric liquids undergoing capillary breakup can lead to accurate measurements of transient extensional rheology of these dilute solutions at relatively low relaxation times (specifically extensional relaxation times in the range $0.01 \leq \tau_E \leq 1s$). This principle is used in the CaBER instrument and has been studied extensively by many researchers [28, 47–49]. When two coaxial cylindrical plates are rapidly separated from each other, a liquid filament will be formed be-

tween the lower and upper liquid reservoirs. The smaller radius of the fluid filament compared to the radius of the two quasi-static reservoirs causes a higher capillary pressure ($\Delta P \sim \sigma/R(t)$) in the connecting ligament. This extra pressure drives an axial flow from the middle of the filament outward to both ends which progressively drains the filament volume into the reservoirs. The driving effect of capillary stresses inside the filament is resisted by either inertia (inertia-capillary regime) or viscous (visco-capillary regime) stresses in a Newtonian liquid. In polymeric solutions the capillary pressure can also be resisted by elastic stresses resulting in an elasto-capillary balance. For different fluid systems and filament dimensions all three effects of inertia, viscous, and elastic stresses may be in balance with the capillary pressure for some part of the thinning and breakup process [24, 47]. For low viscosity fluids in the initial stage of thinning the flow in the filament will be dominated by inertia; and the local diameter will thin down with a timescale set by an inertia-capillary balance (also known as the Rayleigh timescale):

$$\tau_R \equiv \sqrt{\rho R_0^3/\sigma} \tag{6}$$

in which R_0 is the initial radius of the thinning filament. By a simple scaling argument from the balance of capillary pressure with the inertia terms in the equation of motion the time evolution of the filament radius can be derived to be of the form [3, 24] :

$$R(t) = 0.64 \left(\frac{\sigma}{\rho}\right)^{1/3} (1.95\tau_R - t)^{2/3} \tag{7}$$

The predictions from Eq. (7) can be compared with measurements of the thinning filament radius in CaBER at early inertia-capillary stages (see the solid line in Figure 6).

A number of papers (see for example: [46, 47, 50]) have shown that as the filament thins down with time the kinematics of the local flow in the long thin filament evolves into a uniaxial extensional flow [$v_r = (-1/2)\dot{\epsilon}r, v_\theta = 0, v_z = \dot{\epsilon}z$] in which the strain rate is given by $\dot{\epsilon} = (-2/R(t))dR/dt$. The decrease in the diameter results in the strain rate increasing and the corresponding viscous ($\Sigma_{vis} = \eta\dot{\epsilon}$) or elastic ($\Sigma_{elastic} = \eta_E^+\dot{\epsilon}$) stresses in the filament become increasingly important. The viscous forces become significant when the ratio of the visco-capillary time-scale ($t_{vis} \sim \eta R(t)/\sigma$) compared to the inertia-capillary time scale ($t_R \sim \sqrt{\rho R(t)^3/\sigma}$) becomes of order unity, i.e. when the local Ohnesorge number becomes close to one (see also

[24]):

$$Oh \equiv \eta/\sqrt{\rho\sigma R(t)} \sim O(1) \tag{8}$$

Viscoelastic effects can also become significant when the polymer relaxation timescale (τ_E) and the inertio-capillary timescale of the fluid become comparable, i.e. when the local Deborah number is of order unity:

$$De \equiv \tau_E/\sqrt{\rho R(t)^3/\sigma} \sim O(1) \tag{9}$$

Nonlinear growth in the elastic stresses (i.e. strain-hardening) becomes important when the local Weissenberg number $Wi = \tau_E\dot{\epsilon}$ in the filament exceeds $Wi \geq 0.5$.

Bazilevsky et al. [46] showed that for constitutive equations such as the Oldroyd-B model (in which the polymer chains are infinitely extensible) the elasto-capillary region results in an exponential decay of the filament diameter with time of the form:

$$D/D_0 = (GD_0/4\sigma)^{1/3}exp(-t/3\tau_E) \tag{10}$$

where D_0 is the diameter of the filament, σ is the surface tension of liquid-air interface, G is the elastic modulus of the polymer in the solution ($G = nkT$ for a dilute solution) and τ_E is the relaxation time in the Oldroyd-B model for the liquid. Both experiments and theoretical analyses have shown that because the thinning process is self-similar in the elasto-capillary regime the Weissenberg number remains constant with a value equal to $Wi = 2/3$ [47,50].

The exponential decay of the filament diameter in CaBER given by Eq. (10) has been reported by many in the literature for a variety of polymeric liquids used in different applications [17,49,51–53]. However the exponential decay is predicated on infinite extensibility of the polymer chain and as a consequence the thinning filament will never breakup which is, of course, unphysical. Entov and Hinch [50] showed that for constitutive equations which incorporate finite extensibility (such as the FENE-P model for dilute polymer solutions) the elasto-capillary balance and exponential decay in the diameter holds on intermediate timescales but at later times, very close to pinch off, the polymer chains can reach their maximum elongation and the extensional viscosity reaches a plateau. The filament then begins to thin down linearly in a visco-capillary manner once more but with a form given by $D \sim (\sigma/\eta_{E,\infty})(t_b - t)$ where t_b is

the final breakup time.

Figure 5 shows an example of a successful CaBER test performed for a 5000K PEO solution at a concentration $c = 1.5wt.\%$. The montage of images show an axially uniform filament (formed between two hemispherical end-caps) which is thinning with time and the measured diameters are fitted best by an exponential expression for a wide range of times ($200ms \leq t \leq 800ms$ in Figure 5). Regression of Eq. (10) enables a precise measurement for the relaxation time for this solution ($\tau_E \simeq 103ms$). However there are also initial and final regions visible in which the exponential decay does not fit the data anymore. In the initial stage (yellow part of Figure 5, which endures for a few capillary time scales $\sim 6\tau_R$) the polymer chains have not felt the strong stretching flow yet and the balance is between capillarity and a mixture of inertia and viscous forces combined. On the other hand, at long times the polymer chains reach their maximum extensibility so that they can not extend any more and the polymer contribution to the elongational viscosity will saturate. The data in the orange-shaded region of Figure 1 show that the filament diameter deviates from exponential thinning due to finite extensibility and the diameter sharply falls to zero in a linear manner. Also in the final image of the montage in Figure 5 it is possible to observe the so-called "beads-on-a-string structure" [54] at the final stages in which the polymers in the connecting filaments between the beads reach their finite extensibility limit and enter a terminal thinning regime [49].

Ideally every thinning viscoelastic filament would reach an elasto-capillary balance close to pinch off and the CaBER instrument should be able to measure low relaxation times even for very dilute solutions. However there are a number of technical issues which inhibit such measurements [21, 30]. Firstly, it is possible that the relaxation time is so small that the local Deborah number will approach unity only at very low filament diameters that are below the resolution of the laser micrometer in the CaBER. However Rodd et al. [21] showed that the constraint on measurements for CaBER are, in practice, much more severe than the above-mentioned limit. Using a dimensionless map, they showed that measurements become very hard if the values of both initial Deborah and Ohnesorge numbers (based on the initial radius of the sample plates(R_0)) fall below unity. For a $6mm$ diameter plate and an aqueous solution, measurements will be hard if both the relaxation time and the shear viscosity are below $1ms$ and $60mPa.s$ respectively. This restriction is due to the fact that as the end-plates are separated

axially from the initial gap to the final gap there will be shape oscillations in the hemispheri-cal end caps which persist for multiples of the capillary time and these oscillations introduce periodic fluctuations to the laser micrometer readings. If the filament breaks up before these oscillations damp away then the entire life of the thinning filament is corrupted by these end effects. The filament breakup time scales with the larger of the polymer relaxation time (τ_E) or the initial viscous timescale ($t_{vis} = \eta R_0/\sigma$) depending on the magnitude of the elasto-capillary number $Ec \equiv \tau_E \sigma/\eta R_0$. If both of these timescales are shorter than the capillary time-scale of the filament (i.e. $Oh_0 \equiv t_{vis}/\tau_R = \eta/\sqrt{\rho R_0 \sigma} \leq 1$ and also $De_0 \equiv \tau_E/\tau_R = \tau_E/\sqrt{\rho R_0^3/\sigma} \leq 1$) then the filament will break up before the oscillations damp away and the CaBER instrument will fail to report meaningful readings.

Recent work [30, 49] has shown that by modifying the initial rise of the plates to a so-called "slow retraction method (SRM)" the perturbative effects of these inertia-capillary oscillations can be minimized and more accurate measurements are possible for dilute solutions with this new modified approach. However the appearance of the beads-on-a-string structures in CaBER can not be avoided even using the SRM method and Campo-Deaño et al. [30] have proposed following the entire dynamics by high-speed imaging instead of relying on a centrally located laser micrometer read-out alone. An example of a beads-on-a-string structure appearing in a CaBER test with a low viscosity polymer solution is shown in Figure 6. As can be seen from the image montage and from the measured diameter $D(t)$ the initial stage is mainly dominated by an inertia-capillary balance (the solid line fitted to the initial data is the fit from inertia-capillary balance, Eq. (7)) while the rest of the data in the filament thinning region is polluted by the progressive appearance of different generations of beads which appear as the result of an iterated elastic instability [55].

5 Rayleigh-Ohnesorge Jetting Extensional Rheometry (ROJER)

While the new SRM approach described by [30] can enable CaBER measurements for relaxation times down to $240\mu s$, and recent work by Vadillo et al. [31] has described an approach that extends measurements to less than $80\mu s$, there is still a need for alternative instrumentation

that enables facile measurements of low relaxation times for the wide variety of weakly viscoelastic liquids used in many industries such as paint coating, atomization, food and consumer products, inkjet deposition and microfluidic diagnostics used with biopolymeric fluids.

One potential method for probing the elongational properties of a non-Newtonian fluid is to follow the dynamics exhibited during the capillary breakup of a liquid jet. From the pioneering works of Savart [56], Plateau [57] and Rayleigh [58] on the breakup of Newtonian jets there has been a great interest among many researchers in understanding all aspects of this phenomenon [1,59]. Although the nonlinear capillary phenomenon driving jet breakup has motivated many to develop imaging techniques to capture the phenomena [60–62] it has also prompted a few researchers to use the process as a tensiometer for evaluating the surface properties of different liquids [63,64]. Little work focused on non-Newtonian effects until Middleman and coworkers [65–67] studied the effects of viscoelasticity on jet breakup. Their linear stability analysis showed that viscoelastic effects enhance the instability in the linear (small strain) region. This appears to be a counterintuitive result; however, later nonlinear studies [68] showed that while viscoelasticity enhances the initial disturbance growth, in the nonlinear stage the elongation of the polymer chains resist the capillary thinning process and thus the jet will breakup at longer lengths/times compared to Newtonian liquids of comparable shear viscosities. This enhanced resistance of the viscoelastic jet to breakup in the nonlinear region was studied experimentally by Schümmer and Tebel [39,69] by perturbing the jet at set frequencies and capturing the resulting filament thinning behavior with high-speed photographic imaging. Their results showed that it is possible to use measurements of the filament diameter evolution with time in the thinning necks between beads to make estimates of the relaxation time of the fluid using Eq. (10). Later studies by different authors [33,70–73] have further developed the idea of using a thinning viscoelastic jet as an elongational rheometer.

Figure 7 shows the measured data from a jetting experiment performed with a very dilute low molecular weight PEO solution (300K PEO $c/c^* = 0.036$). Snapshots of the jet are captured in both the linear and nonlinear regions at different times (Figure 7(a)). The imposed perturbations at the nozzle lead to the appearance of waves which are advected to the downstream with a velocity equal to the jet velocity (V_j). As the jet travels further away from the nozzle and the amplitude of the wave grows with time, one can select a Lagrangian point (e.g. a point

P at the bottom of a trough) traveling with the jet speed ($Z_P = V_j t$) and record its diameter evolution $D_p(t)$ with time (Figure 7(b)). As we show in Figure 7(b) this capillary thinning of a fixed Lagrangian element can be described in both the linear and non-linear regions. The initial linear variation is a consequence of the growing Rayleigh-Plateau instability and is described by the predictions from linear stability analysis (dashed line in Figure 7(b)):

$$D_P/D_0 = 1 - \delta \, exp(\alpha t) \tag{11}$$

in which δ is the ratio of the imposed initial perturbation to the jet diameter ($\delta \equiv d_{perturbation}/D_0$) and α is the growth rate of the instability derived from the dispersion relation for the Rayleigh-Plateau instability for viscoelastic jets (the details of the linear stability analysis [74] are reviewed in Appendix B).

As the instability grows and the filament diameter decreases further, the local trough evolves into a cylindrical filament with an almost uniform diameter. The values of jet diameter in this nonlinear region no longer agree with linear stability predictions (the dashed line in Figure 7(b)) and the data suggests higher resistance and a slower decay with time compared to the predictions from linear stability analysis. It is also evident that the diameter of the neck decreases in an exponential manner (the solid line fitted to the data is $D_P/D_0 \sim exp(-t/3\tau_E)$). Regression of the data to this expression gives a relaxation time $\tau_E = 60\mu s$. At the same time one can examine the extensional kinematics in the filament and track the values of strain rate with time as shown in Figure 7(c). The strain rate of the Lagrangian element P as it is convected along the jet is given by $\dot{\epsilon}_P \equiv (-2/D_P(t))dD_P/dt$. The value starts to grow with time in the linear region as the material element in the wave trough contracts until the point at which the nonlinear region of deformations ($t \geq 0.6ms$) starts. In the nonlinear region the value of strain rate experienced by the Lagrangian element reaches a plateau at $\dot{\epsilon}_P = 1.1 \times 10^4 s^{-1}$ which corresponds to a constant critical Weissenberg number, $Wi \equiv \tau_E \dot{\epsilon} = 2/3$. These results are in good agreement with both previous experiments and solutions/simulations in the literature for the nonlinear behavior of viscoelastic filaments during the jet breakup [33, 68, 70, 75, 76].

While the agreement of the measured data with the established linear theory of jets is promising, the more important aspect is the ability of ROJER to serve as an elongational rheometer

that can probe very small relaxation times (down to approximately $60\mu s$). There are several advantages in using ROJER for these very dilute solutions compared to a more conventional method such as CaBER; firstly by decreasing the relevant length scale in the instrument from $6mm$ (the plate diameter in CaBER) to the initial nozzle diameter ($2R_0 = 150\mu m$ in RO-JER) the inertio-capillary time-scale is reduced by a factor of almost 250. This means that, in principle, ROJER measurements of material relaxation times are possible for any polymeric solution if the relaxation time is of order of few capillary timescales, which will be $O(10\mu s)$ or higher for the current nozzle size ($\tau_R \sim \sqrt{\rho R_0^3/\sigma} \sim 10\mu s$ for $R_0 = 75\mu m$). This simple geometric modification enables measurements over a wider range of relaxation times and viscosities, for which conventional capillary thinning experiments are unable to properly operate (see [21] for an operation map of CaBER). One may argue that this would have also been possible by decreasing the plate size and consequently the capillary timescale in CaBER but it is important to recognize that in a CaBER device there is an initial stage during which the initial gap opens to the final gap separation, and this distance should be of order of the plate size (D_0) if we expect the capillary column to become unstable and undergo capillary breakup. If this transition does not happen fast enough compared to the speed of capillary thinning then the filament will breakup during the initial separation of the plates and CaBER measurements fail. Thus by simple scaling analysis one will find a lower limit for the speed of the plates in CaBER: $\sqrt{\sigma/\rho D_0} \leq V_{CaBER}$. The required minimum speed for the plate actuator in CaBER becomes very large as the plate radius shrinks and with the current technology on CaBER instruments the rise velocity can not exceed $0.1ms^{-1}$ without positional overshoot issues. This instrumentational limit on the rise speed, dictates a minimum filament diameter below which the filament may breakup during the rise and before the start of measurements ($D_{min} \sim \sigma/\rho V_{CaBER}^2$ which will be around $6mm$ for the a liquid like water and a velocity $V_{CaBER} \sim 0.1ms^{-1}$). Furthermore, decreases in the characteristic radioal length scale of the test sample (from CaBER to ROJER) reduces inertial effects in the fluid and helps us to probe viscoelasticity on much smaller material timescales. Additional benefits in ROJER analysis for very dilute solutions are discussed in the subsequent two sections.

6 Linear Stability Analysis of Viscoelastic Jets and Satellite Drop Formation

The principles of jet extensional rheometry for measuring fluid relaxation times seem fairly straightforward; however there have been many reports in the literature [33, 77, 78] that also describe satellite formation in both Newtonian and viscoelastic jets. The appearance of large satellite droplets must be minimized in ROJER applications as they modify the desired extensional thinning kinematics. Numerical studies by Ardekani et al. [76] explored nonlinear jet thinning and approach to breakup using the Giesekus constitutive equation to describe the complex fluid rheology. They showed that there is a narrow band of wavenumbers for which periodic forcing of the jet will not lead to formation of satellite droplets and this is the optimal range for elongational rheometry. To investigate the appearance of satellite droplets in a representative viscoelastic liquid (a dilute solution of PEO 300K,$c/c^* = 0.03$), a range of different perturbation frequencies (leading to seven different wavenumbers $k_i = 2\pi f_i/V_j$) were picked and the jet breakup was visualized for all different wavenumbers. As expected from theoretical predictions for the inviscid case [32, 58, 79], the results show that the perturbations are linearly unstable and grow with time if the dimensionless wavenumber ($kR_0 \equiv 2\pi f R_0/V_j$) lies between zero and one (i.e. $0 \leq kR_0 \leq 1$). The jet is stable for shorter waves (higher frequency). By fitting a function of the form prescribed by Eq. (11) to the initial data for each wavenumber we can determine the corresponding value of the growth rate (α) and the initial perturbation amplitude (δ) at that wavenumber. The experimental values for the growth rate are plotted at different wavenumbers (blue squares) in Figure 8. The dashed line is a plot of the predictions from the linear theory for the stability of a viscous jet [32], at corresponding values of Ohnesorge number for our tests, and the solid line is a plot of the dispersion curve described by Brenn et al. [74] for the linear stability of a viscoelastic jet at identical conditions to the experiments performed (i.e. equal values of the Deborah, Weber and Ohnesorge numbers). It is worth mentioning that the solid line also includes the effects of the inertia of the external air phase on the jet instability and thus requires specification of the value of the Weber number. As predicted by linear theory for viscoelastic jets [66, 68, 74] the polymer solution is more unstable compared to a viscous Newtonian jet having the same values of the shear viscosity.

The measured values of growth rate in the linear region match very well with the theoretical predictions for the viscoelastic jet.

The fact that the initial stage of the instability is well described by the linear theory can be further appreciated by investigating the final stages of jet breakup when the deformation becomes strongly nonlinear. Since the perturbation of the peizoelectric actuator can be tuned over a wide range of frequencies then at any given velocity for the jet (V_j) we can perturb the jet over a wide range of wavenumbers ($k = 2\pi f_{piezo}/V_j$). This allows us to ensure that the jet is perturbed in the vicinity of its most unstable wavelengths and a monochromatic disturbance will thus grow rapidly with time such that the nonlinear region can be repeatedly imaged with strobe illumination in a periodic manner. Experiments and computations [76] both show that viscoelastic jets tend to generate satellite droplets if the wavenumber is less than the most unstable one (i.e. $kR_0 \leq (kR_0)_{max}$). The size of these satellite droplets decrease as the wavenumber becomes close to $(kR_0)_{max}$ until they finally vanish if the wavenumber exceeds the critical value (the montage of images in Figure 8 illustrate this trend). These observations and computations assist in optimal operation of the jet rheometer and we avoid formation of satellites by perturbing the jet in the narrow band of wavenumbers between the most unstable one and the margin of stability ($(kR_0)_{max} \leq kR_0 \leq 1$). This is essential for precise measurements of rheological material parameters such as fluid relaxation times.

7 Measurements of Relaxation Time

Once the jet is perturbed at the desired frequency we can track the evolution in the filament profile that is contained in a moving Lagrangian box (the red box in Figure 9(a)) that translates downstream with the jet velocity (V_j) so that $Z^{(i)} = Z_0^{(i)} + V_j t^{(i)}$ is the locus of each pixel in the box. The thin translating ligament in the box, which is connected to the two adjacent wave peaks, will have a history identical to a stationary filament in CaBER that connects the two hemispherical end caps to each other. This is illustrated in Figure 9(b) by taking the filament profiles containd in the descending red box shown in Figure 9(a) and arranging them in a time sequence array (time in this figure is equal to the time of flight for the moving Lagrangian box and is simply calculated by $t \equiv z/V_j$). The blue squares in Figure 9(c) show the decay

of the filament in both the linear and the non-linear region. The dashed lines again show the predictions for the exponentially growing perturbation from linear theory:

$$D_{min}/D_0 = 1 - \delta \exp\left[\alpha(De, Oh, We, kR_0)\right] \tag{12}$$

in which the growth rate at the tested conditions (De, Oh, We, kR_0) is directly calculated from the theoretical dispersion relationship coming from the linear stability analysis of Brenn et al. [74] (see appendix B) and the values of δ lie in the range $0.001 \leq \delta \leq 0.01$.

On the other hand the solid line fitted to the data in Figure 9(c) is an exponential fit of the form in Eq. (10). Fitting this model to the data gives us a value of $60\mu s$ for the relaxation time (τ_E). The dynamics of the thinning filament in ROJER are thus identical to the elastocapillary balance established in CaBER and this rheological test can be viewed as a "flying CaBER" which translates downstream with the speed of the jet. The important distinguishing feature of ROJER is the fact that by avoiding the inertia-related issues inherent in CaBER tests we can now measure extremely low relaxation times.

From this analysis it is evident that the externally imposed velocity of the jet serves only as a flow parameter that sets the translation speed of the reference frame. If the ROJER instrument is to be thought of as an extensional rheometer then the analysis must be Galilean-invariant and the measured relaxation times should not depend on the jet velocity. To check this, a series of tests were performed at three different velocities (and consequently different Weber numbers) for the same test fluid (PEO-300K-0.01 wt.%). The results are summarized in Figure 9(c) and one can see that for each test the decay of the filament in the non-linear region matches well with the expected exponential decay and the measured relaxation time for each test is equal to $60 \pm 3\mu s$.

This invariance is expected to be valid over a wide range of Weber numbers. If the imposed jet velocity is in the vicinity of the dripping to jetting transition (i.e. $We_j \leq O(1)$) then the force balance in the thinning filament will be different and the analysis used here must be modified to a new balance which involves the weight of the drop; this has been discussed in detail by Clasen et al. [80]. Conversely, at very high velocities, the aerodynamic forces of the external air column excite the jet to become unstable in different wind-induced modes compared to the

well-known Rayleigh-Plateau mode [81]. This transition happens at gas-phase Weber numbers $(We_{gas} \equiv \rho_{gas}V_j^2/\sigma \approx 0.4)$ which in our experiments with water (for which $\rho_w/\rho_a = 1000$) correspond to liquid-phase Weber numbers higher than $We_j = 400$.

Measurements of relaxation times were also performed for all of the other PEO-based solutions and the resulting values are tabulated in Table 1. Figure 10 shows both a montage of images (Figure 10(a)) and filament diameter data (Figure 10(b)) for two solutions of PEO of different molecular weights (300K and 1000K) but at similar levels of dilution ($c/c^* = 0.36$ for 300K PEO and $c/c^* = 0.37$ for 1000K PEO). The evolutions in the neck diameters in the nonlinear region each show an exponential decay that can be fitted by Eq. (10) (solid lines in Figure 10(b)). As can be seen from the montage of images and the corresponding diameter measurements the lower molecular weight fluid jet (green squares) thins more rapidly, as compared to the higher molecular weight (red triangles). This is reflected in the values of the relaxation times for these two solutions. For the 1000K PEO solution (red triangles) we obtain a value of $\tau_E = 2.8 \times 10^{-3}s$ for the relaxation time, whereas the 300K solution (green squares) at a similar value of c/c^* shows a much lower relaxation time with $\tau_E = 3.6 \times 10^{-4}s$. The longest relaxation time in dilute polymeric solutions can be estimated from the molecular weight of the polymer using Rouse-Zimm theory [82]:

$$\tau_{Zimm} \sim \frac{[\eta]\eta_s M_w}{RT} \tag{13}$$

in which $[\eta]$ is the intrinsic viscosity which is connected to the molecular weight through the Mark-Houwink expression:

$$[\eta] = 0.072 M_w^{3\nu-1} \tag{14}$$

where the solvent quality parameter is $\nu = 0.55$ for PEO solutions in glycerol water mixture [21]. Combining Eqs. (13) and (14) it is apparent that the longest relaxation time for dilute solutions should scale with molecular weight as:

$$\tau_E \sim M_w^{3\nu} \tag{15}$$

This scaling is valid for very dilute solutions ($c/c^* << 1$) but Tirtaatmadja et al. [83] have shown that even at higher (constant) values of c/c^* the dependency on molecular weight remains

similar to Eq. (15). Based on these scaling arguments we expect that for solutions tested in Figure 10(b) the ratio of relaxation times should be: $\tau_{1000K}/\tau_{300K} = (1000/300)^{3 \times 0.55} = 7.30$. The experimental measurements show a ratio of $\tau_{1000K}/\tau_{300K} = 2800/360 = 7.77$, and are thus in good agreement within the expected accuracy of the reported values of solvent quality and polymer molecular weight.

8   Measuring Extensional Properties of Dilute Solutions

To illustrate the capabilities of ROJER, we next focus on studying the effects of the extensional viscosity on the atomization of different dilute polymer solutions, as illustrated in Figure 11. Measurements of the steady shear viscosity do not show any significant difference between the tested solutions but ROJER visualization of the filament thinning dynamics with time do show a significant change even for very dilute solutions. This difference can be detected by comparing the evolution in filament diameter for a fixed material element in the viscoelastic liquid (red filled circles in Figure 11(c)) with the corresponding Newtonian solvent (blue open circles in Figure 11(c)). This difference in thinning can be quantified, as discussed in detail in previous sections, by fitting the exponential decay in the viscoelastic case (black solid line in Figure 11(c)) and the linear visco-capillary thinning observed in the solvent (dashed line in Figure 11(c)). From the fits one can evaluate the values of strain rate and the tensile stress difference in the thinning material element from the following expressions [47]:

$$\dot{\epsilon}_P = \frac{-2}{D_P(t)} \frac{dD_P(t)}{dt} \tag{16a}$$

$$\Delta\Sigma(t) = \Sigma_{zz} - \Sigma_{rr} = 2\sigma/D_P(t), \tag{16b}$$

Using the relationships in Eqs. (16a) and (16b) explicit relationships can be found for the time-varying apparent elongational viscosity in the thinning jet:

$$\eta_E^+ \equiv \frac{\Sigma_{zz} - \Sigma_{rr}}{\dot{\epsilon}_P} = \frac{-\sigma}{dD_P(t)/dt} \tag{17}$$

From this expression it is apparent that by measuring the evolution in the filament diameter with time for a fixed material point P we can calculate both the strain rate and the instanta-

neous elongational viscosity at that specific strain rate. Using the ROJER data from Figure 11(c) the corresponding values of elongational viscosity are calculated and plotted versus strain rate for the PEO-300K-0.01 wt.% fluid. Figure 11(d) shows a comparison between the shear (triangles) and elongational (circles) viscosity for the viscoelastic solution (red filled symbols) and the Newtonian solvent (blue open symbols). The shear viscosity shows negligible increase with addition of dissolved polymer and no dependence on shear rate; by contrast there is a considerable increase in the extensional viscosity of the PEO solution. The Newtonian solvent shows a constant value of elongational viscosity equal to $3\eta_s$ which is is in agreement with the expected Trouton ratio for Newtonian liquids [42]. The PEO solution shows very similar values of the elongational viscosity to the solvent at low strain rates, but then starts to increase when the strain rate approaches a critical value, which is close to the relaxation rate of the polymer chains in the elongational flow (τ_E^{-1}). The Weissenberg number of the flow at this point corresponds to the coil to stretch transition for the dissolved polymer chains, $Wi = \tau_E \dot{\epsilon} \simeq 0.5$ [84]. The experimental results for the PEO solution also show good agreement with the FENE-P (finite extensibility nonlinear elastic dumbbell) model proposed by Peterlin [84, 85] in both shear (dashed line in Figure 11(d)) and extension (solid line in Figure 11(d)). The parameters used in evaluating the predictions of the FENE-P model are the measured values of zero shear viscosity (η_0), the solvent viscosity (η_s) and the relaxation time (τ_E) along with the extensibility parameter $(L \simeq 27)$ which is computed from the known molecular parameters for the PEO chains [37]. The FENE-P model predicts negligible change in the shear viscosity for the dilute solution but a considerable increase in the extensional viscosity for $Wi \geq 0.5$. Due to the nonlinear nature of the FENE springs the extension of the individual polymer chains are constrained by the extensibility parameter (L). Once fully extended the chains act like an anisotropic suspension of rigid rods and the extensional viscosity in the bulk reaches a plateau value at high strain rates $(\lim_{\tau_E \dot{\epsilon} \gg 1} \eta_E \to 3\eta_s + 2(\eta_0 - \eta_s) L^2)$.

The enhanced resistance of the viscoelastic solution to stretching in elongational flows plays a key role in controlling the dynamics of the filaments close to the breakup point from the rapidly deforming liquid core during the atomization process (see Figure 1(b and d)). This additional resistance leads to the appearance of elongated filaments connecting the large beads to each other. A signature of this effect can be seen by looking at snapshots of the atomized

droplets in any ligament-mediated atomization process such as those shown in Figure 11(a). Images of the atomized viscoelastic liquid sample always show greater numbers of both large and small droplets compared to the Newtonian solutions (compare Figures 11(a) and 11(b)); i.e. the droplet size distribution is changed due to the extensional rheology of the test fluid. To explore the effects of viscoelasticity we next calculate the first moment of this size distribution to understand how the average droplet size $< d >$ depends on the intrinsic Deborah number of the test fluid.

9   Effect of Extensional Properties on Atomization

As noted in the introduction, the increase in the average droplet size observed during atomization of viscoelastic liquids is a key feature that has been observed by many previous authors in the literature [4, 15, 18, 72, 86–88] but most previous attempts to connect this increase with the fluid relaxation timescale have not been very successful [4, 18, 72, 87]. This has been primarily due to the fact that the proposed models can not capture one other key feature, which is the saturation of the effect at large values of the relaxation time. Previous analyses have argued that the droplet average size should be proportional to the wavelength of the final instability process during the atomization event, and a combination of linear stability analyses for the different instability modes in the air spray should predict the measured values for the mean droplet diameter $< d >$[2, 89]. Although this scaling may work for inviscid jets, recent work by Marmottant and Villermaux [3] for viscous Newtonian fluids shows that the effects of viscosity on the lifetime of the ligaments that form in the final stages of detachment from the core liquid jet play a dominant role in setting the average droplet size in the spray. In their tests, Marmottant and Villermaux showed that by increasing the Newtonian viscosity of the atomized fluid, the thinning neck that connects elongating ligaments to the core liquid jet will have more time to breakup. This viscous retardation of the capillary thinning and breakup process enables the filament to uniformly elongate into the surrounding air phase due to the external shear stresses exerted by the air stream. This additional extension reduces the thickness of the ligament (which controls the average droplet size following breakup). More viscous liquids thus form longer and thinner filaments, which also agrees with our common experience of long and thin

syrup filaments that arise when we pour such liquids from relatively high heights. During this thinning process the volume of the filament remains constant (and equal to the initial volume) i.e. $V(t) = V_0 \sim d_l^3$. What Marmottant and Villermaux [3] show can be summarized in the following scaling for the average droplet sizes based on the breakup time of the neck of the filament:

$$< d > /d_l \simeq t_a/t_b \qquad (18)$$

in which d_l is the initial characteristic size of the ligament before the elongation process, t_b is the breakup time of the neck of the filament and $t_a \equiv (d_l/u_{air})(\rho_{liquid}/\rho_{air})^{1/2}$ is a characteristic timescale for the acceleration arising from the air dragging the ligament away from the core liquid jet. Eq. (18) shows that the average diameter and the neck breakup time are inversely proportional since the viscous fluid ligament will continue to uniformly stretch while the neck is thinning with time.

In order to understand this mechanism better, especially for viscoelastic solutions, we consider the experiment shown in Figure 12, which is designed to emulate sudden extensional effects in the spray. Viscoelastic liquid samples with fixed initial volume (V_0) were placed between the two plates of the CaBER and the two plates were separated from each other at relatively high strain rates to mimic the fast extensional action of the airstream during the ligament stretching and subsequent atomization phenomena. A similar configuration has been used by Villermaux and his coworkers in mimicking fragmentation processes for Newtonian fluids [3, 90].

To analyze the effects of viscoelasticity on the average droplet sizes, a simple scaling model which is similar to the one used by Marmottant and Villermaux [3], is introduced in Appendix C. The new model, using the observations from the step stretch experiment, gives a scaling for the average droplet size observed in air-assisted atomization of viscoelastic liquids:

$$\frac{< d >_{VE}}{< d >_N} = \frac{(\sqrt{8}c/6)Oh_{R_l}^{-1} + Oh_{R_l}^2}{(\sqrt{8}c/6)Oh_{R_l}^{-1} + Oh_{R_l}^2 - \ln\left(1 + cDe_{R_l}/3Oh_{R_l}\right)} \qquad (19)$$

Details of the analysis are discussed in appendix C. The single unknown constant c in this analysis is expected to be of order unity.

Marmottant and Villermaux [3] have shown that for a Newtonian liquid measured average diameter and the initial ligament scale d_l are related by: $< d > /d_l = We_{d_l}^{-1/2} = \left(\sigma/\rho u_{air}^2 d_l\right)^{1/2}$.

Using this expression and the measured value of average droplet size $,< d >_N$, for a Newtonian liquid at a typical air speed of $u_{air} \simeq 100ms^{-1}$ we can evaluate the ligament size as $d_l = 2R_l \simeq 170\mu m$. Because elastic effects are unimportant at early stages we assume this value is unchanged for the weakly elastic polymer solutions. We can plot the evolution in this scaling model prediction (Eq. (19)) for different relaxation times (τ_E) measured using ROJER and compare the model with the experimentally measured sizes from atomization tests. The solid line in Figure 12 (b) shows the theoretical predictions from this simple model (with the constant $c = 4.1$) compared with the measured average sizes for the tested viscoelastic solutions normalized by the corresponding value for the Newtonian solvent under identical conditions $< d >_N= 16\mu m$. The model captures very well both the initial increase of sizes at low intrinsic Deborah numbers (based on the length scale of the elongated ligament $De_{R_l} = \tau_E/\sqrt{\rho R_l^3/\sigma}$) and also the saturation observed at higher De_{R_l}. The same plot with a linear ordinate axis and a logarithmic abscissa is shown as the inset image in Figure 12 (b) and it is clear that the average drop size changes approximately linearly with $\ln(De)$. For the cases considered here $\tau_R = \sqrt{\rho R_l^3/\sigma} = 101\mu s, \tau_{vis} = 4\mu s$ and $Oh_{R_l} = 0.04$. Even for a maximum fluid relaxation time of $6000\mu s$, the logarithmic term is smaller than the initial terms $\left((\sqrt{8}c/6)Oh_{R_l}^{-1} + Oh_{R_l}^2\right)$ in the denominator, and thus the expression in Eq. (19) can be Taylor-expanded as:

$$\frac{< d >_{VE}}{< d >_N} \simeq 1 + \frac{\ln\left(1 + cDe_{R_l}/3Oh_{R_l}\right)}{(\sqrt{8}c/6)Oh_{R_l}^{-1} + Oh_{R_l}^2} \tag{20}$$

which in the limit of $cDe_{R_l}/3Oh_{R_l} \gg 1$ is equivalent to a linear dependency of the mean drop size $< d >$ on $\ln(De_l)$ ($1.9 \leq cDe_{R_l}/3Oh_{R_l} \leq 92.6$ in our tests) which is in good agreement with our experimental observations.

10 Conclusions

We have shown that a periodically forced viscoelastic jet combined with a strobe-based digital video imaging system can form the basis of an extensional rheometer that is suitable for studying weakly viscoelastic fluids. Operation of this jetting rheometer requires an understanding of the interplay of viscous, inertial and elastic forces in the jet and we therefore refer to this as a Rayleigh-Ohnesorge Jet Extensional Rheometer (ROJER).

The shear and extensional rheology of several dilute PEO solutions were studied using the ROJER. Flow visualization studies of the performance of these fluids in air-assisted atomization were also performed. The shear rheology of these dilute polymeric solutions did not suggest any significant difference in their atomization performance whereas both the flow visualization and drop diameter measurements from our spray tests showed an increase in the mean drop size. The extensional rheology for these solutions was measured using both CaBER and ROJER and we showed that due to the inertia-capillary timescale there is a lower limit for measurements of relaxation times in a CaBER device. This limit can be circumvented by studying the dynamics of capillary breakup using the ROJER device because of the much smaller length and time scales involved. Measurements obtained from ROJER in terms of both linear stability and nonlinear elasto-capillary thinning analysis of the jet were verified using known theoretical and numerical predictions and it was shown that quantitative agreement can be obtained with existing stability theory. The values of relaxation times extracted from this analysis were used to quantify the performance of the test fluids in the air-assisted atomization process. Using our observations, a new and relatively simple model was developed for understanding the viscoelastic dynamics of the ligament thinning process close to their final detachment from the core liquid jet. Using the measured relaxation times within the framework of the suggested model a physical prediction for the average droplet size $< d >_{VE}$ during atomization of a weakly viscoelastic fluid was obtained and the experimental results with four different PEO solutions were found to agree well with the model predictions.

This study helps us understand the subtle effect of extensional rheology on the breakup and the atomization of weakly viscoelastic liquids which are widely used in many biological and industrial applications. For Newtonian liquids, two different scalings for ligament sizes are suggested based on linear stability analysis [89, 91]. The difference between the two scalings arises from the Rayleigh Taylor stability analysis, in which the direction of air acceleration relative to the liquid/air interface can change at different air/liquid flow rate ratios. The competing effect of viscosity and surface tension on the average droplet size in an air atomizer can be understood by a simplified version of the original scaling from Aliseda et al. [89]:

$$\frac{d_l}{D_0} \simeq 1.2 \left(\frac{\sigma}{\rho u_{air}^2 D_0} \right)^{1/2} \left[1 + We^{1/6} Oh^{2/3} \right] \tag{21}$$

where d_l is the size of ligament being accelerated away from the jet and the Weber and Ohnesorge numbers in Eq. (21) are calculated based on the diameter of the nozzle D_0.

Marmottant and Villermaux [3] have shown that due to the viscous slowing of the filament break up, viscous Newtonian filaments stretch more than inviscid ligaments do in the air stream. Using a similar approach to the analysis carried out in Appendix C one can suggest a scaling for the average droplet size for the atomization of viscous Newtonian liquids:

$$\frac{<d>_N}{d_l} = \frac{(\sqrt{8}c/6)Oh_{R_l}^{-1}}{(\sqrt{8}c/6)Oh_{R_l}^{-1} + Oh_{R_l}^2} = \frac{(\sqrt{8}c/6)}{(\sqrt{8}c/6) + Oh_{R_l}^3} \tag{22}$$

where now the value of the Ohnesorge number is based on the characteristic length scale in the ligament. We also have shown how the final average droplet size and the ligament thickness d_l is modified in the presence of weak fluid elasticity through a result of the form shown in Eq. (19). This expression is found to agree well with our experimental measurements for a number of PEO solutions.

The simplest way to include all of the competing effects of viscosity, surface tension and elasticity on overall mean droplet sizes is by combining Eqs. (21), (22) and (19) which results in an expression of the form:

$$\frac{<d>_{VE}}{D_0} \simeq 1.2 \left(\frac{\sigma}{\rho u_{air}^2 D_0}\right)^{1/2} \left[1 + We^{1/6}Oh^{2/3}\right] \left[\frac{(\sqrt{8}c/6)Oh_{R_l}^{-1}}{(\sqrt{8}c/6)Oh_{R_l}^{-1} + Oh_{R_l}^2 - \ln\left(1 + cDe_{R_l}/3Oh_{R_l}\right)}\right] \tag{23}$$

This suggested scaling is the first attempt to address in a complete way the different effects of fluid viscosity and elongational relaxation time on the average droplet size produced in air atomization for weakly viscoelastic solutions. The model incorporates all of the essential fluid properties and geometry dimensions. Quantitative predictions from this model agree well with experimental results for the four tested PEO solutions. A similar combination of classical linear stability theory, scaling arguments and benchmark experiments were used by Middleman and coworkers [65,66] to systematically understand the effects of surface tension, viscosity and weak elasticity on the breakup length of viscoelastic jets. Jet rheometry of mobile liquids using the ROJER instrumentation thus provides a pathway to realize the concept originally outlined by Walters some 30 years ago of "...a flow dominated by extension that can be analyzed in

a quantitative fashion to extract material functions that are rheologically meaningful". The rheologically meaningful functions here are the extensional relaxation time $\tau_E(c, M_w)$ and the instantaneous apparent Trouton ratio $\eta_E^+ (\dot{\epsilon}, t) / \eta_0$. We have demonstrated that quantitative measurements of relaxation times as small as $60 \mu s$ can help us understand the key role of nonlinear viscoelasticity in modifying the mean droplet size in an air-assisted atomization process. It will be of interest to see if these rheological properties can also help understand other features of this important industrial process such as changes in the shape and breadth of the droplet size distribution in the final spray fan.

11   Acknowledgments

Appendix

A   Deriving the Strobe Factor

If a motion is periodic with a characteristic frequency f then with a suitable choice of initial time to specify the phase the position of the object $x(t)$ can be described by:

$$x(t) = A_0 \sin(2\pi f t) \tag{24}$$

where A_0 is the amplitude of oscillation. The velocity of the object at a given time t_0 can be derived by differentiating $x(t)$ with respect to time:

$$V_r(t_0) = 2\pi f A_0 \cos(2\pi f t_0) \tag{25}$$

Now when the observer is monitoring the motion with a prescribed frequency close to f (e.g. the frequency of a strobe light pulsed at a frequency close to f) the apparent velocity calculated from observation of the point of two consecutive instants in time to the observer will be different from the real velocity. Lets say that the observer is tracking the object displacement with a frequency $f_{obs} = f - \Delta f$ then the apparent motion from time t_0 to $t_0 + \delta t$ in which $\delta t = 1/f_{obs} = 1/(f - \Delta f)$ will be:

$$x(t_0 + \delta t) - x(t_0) = A_0 \left[\sin\left(2\pi f(t_0 + \delta t)\right) - \sin(2\pi f t_0) \right] \tag{26}$$

which can be expanded to:

$$A_0 \left[\sin(2\pi f t_0) \cos(2\pi f \delta t) + \cos(2\pi f t_0) \sin(2\pi f \delta t) - \sin(2\pi f t_0) \right] \tag{27}$$

In the limit of $\Delta f / f << 1$ it can be shown by Taylor expansion of the trigonometric terms in Eq. (27) that to first order in $\Delta f / f$:

$$\sin\left(2\pi f \delta t\right) \simeq 2\pi(\Delta f / f)$$
$$\cos\left(2\pi f \delta t\right) \simeq 1 \tag{28}$$

thus the relative apparent motion for th observer can be estimated as:

$$x(t_0 + \delta t) - x(t_0) \simeq 2\pi A_0 (\Delta f / f) \cos(2\pi f t_0) \tag{29}$$

from which the apparent velocity can be calculated by:

$$V_{app}(t_0) = \frac{x(t_0 + \delta t) - x(t_0)}{\delta t} \sim 2\pi \Delta f A_0 \cos(2\pi f t_0) \tag{30}$$

Comparing the result for apparent velocity from Eq. (30) with the real velocity from Eq. (25) shows that the apparent motions seems slower than the real one by a factor equal to $\Delta f / f$.

B   Details of the Linear Stability Analysis

Brenn et al. [74] derived the dispersion curve for an axisymmetric viscoelastic jet using corotational Oldroyd eight constant model as the constitutive equation [16]. We retain only the terms that give the Oldroyd-B model. After linearizing the governing equations for conservation of mass and momentum in cylindrical coordinates and applying the right kinematic and dynamic boundary conditions at the liquid/air interface, Brenn et al. [74] show that the following dispersion relation can be derived for the linear stability of the jet:

$$
\begin{aligned}
&\Omega_r^2 \frac{kR_0}{2} \left[\frac{I_0(kR_0)}{I_1(kR_0)} + \frac{\rho_g}{\rho_l} \frac{K_0(kR_0)}{K_1(kR_0)} \right] + \Omega_r (kR_0)^2 Oh \frac{1 + (\lambda_2/\lambda_1) De\Omega_r}{1 + 1 De\Omega_r} \times \\
&\left[2kR_0 \frac{I_0(kR_0)}{I_1(kR_0)} \left(1 + (kR_0)^2 \frac{Oh}{\Omega_r} \frac{1 + (\lambda_2/\lambda_1) De\Omega_r}{1 + De\Omega_r} \right) - 1 - 2lR_0 \frac{I_0(lR_0)}{I_1(lR_0)} (kR_0)^2 \frac{Oh}{\Omega_r} \frac{1 + (\lambda_2/\lambda_1) De\Omega_r}{1 + De\Omega_r} \right] \\
&= \frac{(kR_0)^2}{2} \left(1 - (kR_0)^2 \right) + C \frac{\rho_g}{\rho_l} \frac{k^3}{R_0^3} We \frac{K_0(kR_0)}{K_1(kR_0)}
\end{aligned}
\tag{31}
$$

in which $\Omega_r = \alpha_r \tau_R$ is the dimensionless growth rate (scales with the capillary timescale $\tau_R \equiv \sqrt{\rho_l R_0^3/\sigma}$), kR_0 is the dimensionless wavenumber, ρ_g and ρ_l are respectively the gas and liquid density, $Oh = \eta_0/\sqrt{\rho_l \sigma R_0}$ is the Ohnesorge number, $De = \lambda_1/\sqrt{\rho_l R_0^3/\sigma}$ is the Deborah number, I_n and K_n are the modified Bessel functions, λ_2 is the retardation time $\lambda_2 = \eta_s \lambda_1/\eta_0$ and λ_1 is the relaxation time in the Oldroyd-B model. The constant C is an empirical correction factor to incorporate the aerodynamic forces on the jet and has a constant value of $C = 0.175$

according to [74]. Here l is a modified wavenumber defined as:

$$l^2 \equiv k^2 + \frac{\rho(\alpha + ikV_j)}{\eta(\alpha)} \tag{32}$$

where $\alpha = \alpha_r + i\alpha_i$ is the (complex) growth rate and:

$$\eta(\alpha) = \eta_0 \frac{1 + \lambda_2(\alpha + ikV_j)}{1 + \lambda_1(\alpha + ikV_j)} \tag{33}$$

The dispersion relation shown in Eq. (31) incorporates the effects of the air/gas flow in the vicinity of the jet and the results converge to the stability analysis carried out by Goldin et al. [75] in the limit of zero air/gas effect, i.e. when ρ_g goes to 0.

Eq. (32) is a nonlinear dispersion relation and at fixed values of De, Oh, We and for a given value of k the root which is $\Omega_r = \alpha_r \tau_R$ can be found using a simple numerical solver in Matlab. Results at different values of kR_0 are plotted and compared with measurements in Figure 8 (black solid line).

C Analysis of the Effects of Relaxation Time on Average Droplet Size in a Viscoelastic Spray

As discussed in Section 9 in order to emulate the dynamics of ligaments close to pinch off in the atomization process (see Figure C.1(a) and C.1(b)) a sudden "step-stretch" test has been devised using the CaBER platform in conjunction with high speed video image analysis. In this test we impose a very rapid axial displacement of the upper plate in the CaBER device. Because of fluid inertial effects, the liquid sample cannot respond rapidly enough to form a uniform liquid bridge. This may preclude analysis of the self-similar capillary thinning required in CaBER analysis, but it closely emulates the rapid formation and acceleration of fluid ligament that can be seen in the jet image shown in Figure C.1(a). This process has been considered in detail by Marmottant and Villermaux [3] for Newtonian fluids, and we follow their analysis for viscoelastic fluid ligaments. Specially we observe the formation of a primary or main ligament $L_{ligament}(t)$ (or $L_{CaBER}(t)$ in our replicated experiment) that is connected by a thinning neck region (of diameter $2r_n^{CaBER}(t)$) to the primary drop (or hemispherical end-cap region in our

replicated experiment). Figures C.1(c) and 12(a) in the main text show a montage of images for a step stretch test with the 300K-PEO-0.01 wt.% solution. For an inviscid fluid, Marmottant and Villermaux [3] show that the lifetime of this neck is independent of the stretch rate and depends only on the inertio-capillary timescale of the initial ligament. In our notation (based on radius rather than diameter) this lifetime is $\sim \sqrt{8}\tau_R$ (see Figure 13 in [3]).

Repeating the test for different viscoelastic solutions shows that in all of the step-stretch tests the additional viscoelasticity increases the lifetime of the neck region and the neck clearly forms an elongated microfilament close to its pinch off (see for example the image at $t = 23.3ms$ in the test). This means that the local flow in the neck must reach a critical strain rate close to break up that corresponds to a critical Weissenberg number of $Wi \sim O(1)$. The interesting result from our video imaging observations is the fact that before reaching this critical Weisenberg number the neck contributes little to the overall force balance and serves principally to maintain the integrity of the primary ligament fixed at the bottom/top. In the early images of Figure C.1(c) (i.e. for times $t \leq 23ms$) it is clear that the primary ligament continues to stretch (i.e. $dL_{CaBER}/dt > 0$). However when the neck suddenly pinches down, and the extensional flow in the neck reaches the critical Weissenberg number, the main ligament is effectively isolated from the deformation being imposed at the end plates. The main ligament no longer elongates (i.e. $dL_{CaBER}/dt \to 0$). A capillary wave now starts to propagate along the isolated ligament and leads to an increasingly corrugated shape that eventually fragments into droplets. This result, repeatable over many tests, is distinctly different than observations for viscous Newtonian liquids, in which the main ligament and the thin connecting neck both thin down continuously under a visco-capillary balance such that the extensional deformation is a rather uniform process along the ligament axis. By contrast for viscoelastic solutions, when the local flow inside the neck reaches an elasto-capillary balance then the resulting deformation is located in the (very thin) neck, rather than in the primary ligament, and the main body of the ligament will experience negligible subsequent deformation.
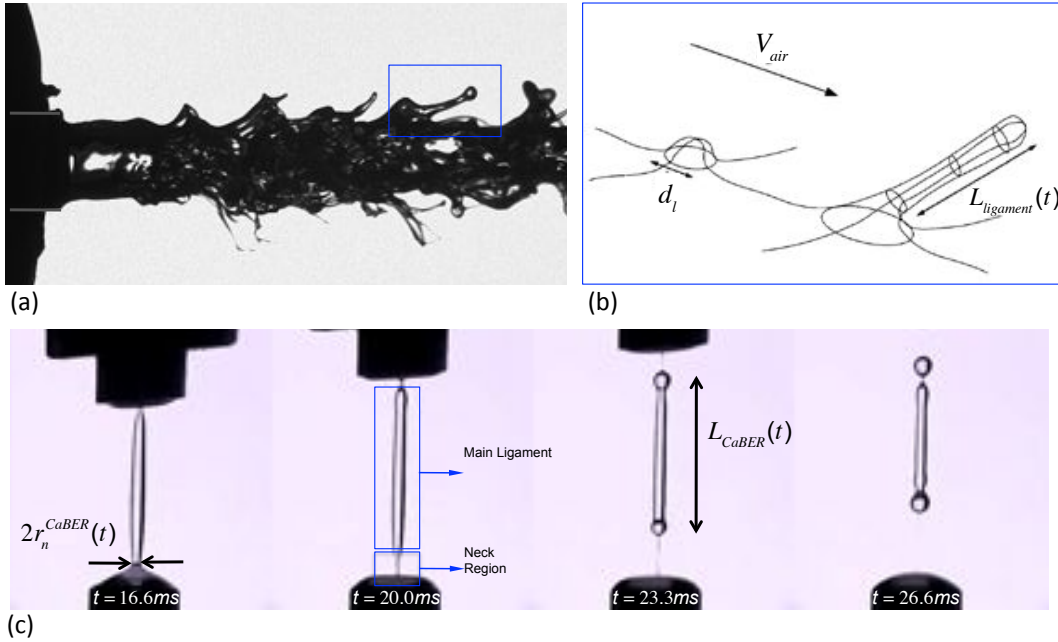
Figure C. 1: (a) Spray visualization image for the viscoelastic polymer solution (PEO-300K-0.01 wt.% in solvent) close to the nozzle. A ligament can be seen in the blue box which is elongated by the air stream (b) Schematic of the suggested model by Marmottant and Villermaux [3] for analyzing the dynamics of the ligament, (reproduced with permission). (c) Montage of images from sudden step-extension test for the viscoelastic solution (PEO-300K-0.01 wt.% in the solvent) in a CaBER instrument. As soon as the flow in the neck region reaches the elasto-capillary balance ($t \geq 20.0ms$) subsequent deformation is localized in the neck while the main ligament stops stretching ($dL_{CaBER}/dt \simeq 0$) and a capillary wave propagates along the filament.

To understand the effect of this sudden cessation of the stretching in the main ligament on the average diameters of droplets formed in the spray in a quantitative way we need to analyze the local flow in the neck more accurately. We assume that close to pinch-off, fluid inertia will be negligible compared to viscous effects and we start our analysis before the flow in the filament reaches the elasto-capillary region (i.e. we start from the onset of a visco-capillary pinch). The flow in the thinning neck will be a simple force balance between the viscous and capillary stresses:

$$-3\eta \frac{2}{r(t)} \frac{dr(t)}{dt} = c\sigma \left(\frac{1}{r(t)} - \frac{1}{R_l} \right) \qquad (34)$$

in which $r(t)$ is the local midpoint radius of the thinning neck and $R_l = d_l/2$ is the radius of the initial volume of fluid ligament undergoing the stretch. In this process the local neck is not (at

first) a long cylindrical filament in which we can simply assume that the two principal radii of curvature are $R_1 = r(t)$ and $R_2 \to \infty$ but instead is a short neck connected to a hemispherical reservoir (or droplet) with radius of R_l at the base; we therefore take the radii of curvature as $R_1 = r(t)$ and $R_2 = -R_l$ respectively. The coefficient of proportionality appearing in Eq. (19) is expected to be of order of unity. In their original analysis Entov and Hinch [50] take $c = 1$ and in the limit of long thin filaments ($r/R_l << 1$) the self-similarity solution or viscocapillary thinning derived by Papageorgiou gives $c = 0.42$ [92]. We retain c as a single fitting constant in our subsequent analysis. Integrating Eq. (34) yields an evolution equation for the diameter of the neck in the visco-capillary region:

$$\frac{r}{R_l} = 1 - exp\left(\frac{c}{6\tau_{vis}}\left(t - t_b^{(VC)}\right)\right) \tag{35}$$

in which τ_{vis} is the characteristic visco-capillary timescale $\tau_{vis} = \eta R_l/\sigma$ and the visco-capillary breakup time is shown as $t_b^{(VC)}$. In order to find an estimated value for the breakup time $t_b^{(VC)}$, we only need to have a physical estimate for the radius at the start of the visco-capillary region $r(t = 0)/R_l$. Eggers and Villermaux [1] have shown that the visco-capillary region starts when the local Ohnesorge number ($\eta/\sqrt{\rho\sigma r(t)}$) becomes of order unity and using this assumption the value of $r(t = 0)/R_l$ can be estimated to be around $\eta^2/\rho\sigma R_l$, thus one can find a meaningful estimate for the breakup time of the ligament in the visco-capillary regime:

$$t_b^{(VC)} = -\frac{6\tau_{vis}}{c}ln\left(1 - Oh_{R_l}^2\right) \sim \frac{6\tau_{vis}Oh_{R_l}^2}{c} \tag{36}$$

in which Oh_{R_l} is the initial(small) value of the Ohnesorge number based on the initial size of the fluid ligament:

$$Oh_{R_l} \equiv \frac{\eta}{\sqrt{\rho\sigma R_l}} \ll 1 \tag{37}$$

As a side note, by Taylor series expansion of Eq. (35), we can investigate the predictions of the suggested model in the limit of times close to the break up ($t_b^{(VC)} - t) \to 0$ or equivalently from a geometrical viewpoint in the limit of small values of $r(t)/R_l$:

$$\frac{r(t)}{R_l} = 1 - \left(1 + \frac{c}{6\tau_{vis}}\left(t - t_b^{(VC)}\right) + ...\right) \simeq \frac{c}{6\tau_{vis}}\left(t_b^{(VC)} - t\right) \tag{38}$$

This expression shows that the proposed scaling model leads, in the limit of thin and slender neck region ($r(t)/R_l \ll 1$), to the expected similarity solution for viscocapillary thinning of Newtonian slender filaments [92–94].

The addition of viscoelasticity has a significant effect on this process, as shown in the montage of images presented in Figure 12(a). The main ligament in the viscoelastic filament stops stretching after the neck locally attains an elasto-capillary balance and the bulk of the remaining deformation is localized in the thin neck after that point. The criterion for onset of this process can be estimated by comparing the strength of the flow in the filament neck ($\sim \dot{\epsilon}_{neck}$) to the relaxation time of the liquid; when $Wi_{neck} \equiv \tau_e \dot{\epsilon}_{neck} \sim O(1)$ the polymer chains are extended faster than the rate at which they can relax. Elastic stresses will therefore dominate and grow and arrest the pinch-off process. The subsequent deformation happens primarily in the neck while being arrested in the main ligament (which will now undergo capillary recoil and formation of a satellite drop). To find an estimate for the starting time of the elasto-capillary region in the neck we use the visco-capillary model obtained above (Eq. (35)) and follow the evolving strain rate; the stretching in the main ligament stops when the value of the strain rate in the connecting neck reaches a critical value close to the relaxation rate of the polymer i.e. the time at which $\dot{\epsilon}_{neck} \sim 1/\tau_E$. If we denote this time by $t_{pinch}^{(EC)}$ using Eq. (35) then we can find an expression for the strain rate from which $t_{pinch}^{(EC)}$ can be evaluated as a function of relaxation time (τ_E) and other parameters in the model:

$$t_{pinch}^{(EC)} = t_b^{(VC)} - \frac{6\tau_{vis}}{c} \ln \left(1 + \frac{c\tau_E}{3\tau_{vis}} \right) \tag{39}$$

The addition of viscoelasticity (i.e. nonzero values of τ_E) thus reduces the critical time ($t_{pinch}^{(EC)}$) at which the flow in the neck attains an elasto-capillary balance; consequently the span of time for which the main ligament is stretching in the air will be reduced. If the lifetime of the thinning filament for a viscous Newtonian fluid is estimated as $\sqrt{8}\tau_R + t_b^{(VC)}$ where $\sqrt{8}\tau_R$ is the initial time required for the flow in the neck to reach the visco-capillary balance (as shown by Marmottant and Villermaux [3] this initial time is set purely by the inertio-capillary timescale since in this initial stage inertial and capillary stresses are the dominant ones in balance) then the new (reduced) lifetime become $\sqrt{8}\tau_R + t_{pinch}^{(EC)}$ for viscoelastic solutions.

Less stretching leads to shorter and thicker viscoelastic ligaments which will end up breaking up into bigger (average size) droplets. This trend agrees with the qualitative observations of average sizes in the atomization of viscoelastic liquids shown in Figure 12(b). For a more quantitative comparison we combine Eqs. (18), (37) and (40) to obtain the following expression for the effect of fluid elasticity on the average drop sizes:

$$\frac{<d>_{VE}}{<d>_N} = \frac{(\sqrt{8}c/6)\tau_R + \tau_{vis.}Oh^2_{R_l}}{(\sqrt{8}c/6)\tau_R + \tau_{vis.}Oh^2_{R_l} - \tau_{vis}\ln\left(1 + c\tau_E/3\tau_{vis}\right)} \tag{40}$$

where $<d>_{VE}$ denotes the average droplet size in the viscoelastic spray and $<d>_N$ denotes the corresponding value for a Newtonian spray.

Eq. (41) can be further simplified into a form that only incorporates the dimensionless Ohnesorge and Deborah numbers with $c = 4.1$ as a fitting parameter:

$$\frac{<d>_{VE}}{<d>_N} = \frac{(\sqrt{8}c/6)Oh^{-1}_{R_l} + Oh^2_{R_l}}{(\sqrt{8}c/6)Oh^{-1}_{R_l} + Oh^2_{R_l} - \ln\left(1 + cDe_{R_l}/3Oh_{R_l}\right)} \tag{41}$$

Table 1: Rheological properties of the viscoelastic test fluids. Two different concentrations of Poly(ethylene oxide) (PEO) at two different molecular weights were dissolved in the Newtonian solvent (Water+Glycerol 60-40 wt.%) which has a viscosity $\eta_s = 3.2 mPa.s$. The dimensionless parameters Oh and De are defined in the text (see Eqs. (8) and (9)) and are evaluated using $\rho = 1103 kg/m^3$ and $R_l = 85\mu m$.

Mw	c	c/c^*	$\eta_0[mPa.s]$	$\tau_E[\mu s]$	L	De	Oh
300K	0.01%	0.036	3.21	60	27	0.2	0.04
300K	0.1%	0.36	3.32	360	27	1.3	0.04
1000K	0.01%	0.07	3.22	996	50	3.6	0.04
1000K	0.05%	0.37	3.31	2800	50	10.0	0.04

(a) Newtonian solvent close to the nozzle

(c) Newtonian solvent far from the nozzle

(b) PEO solution close to the nozzle

(d) PEO solution far from the nozzle
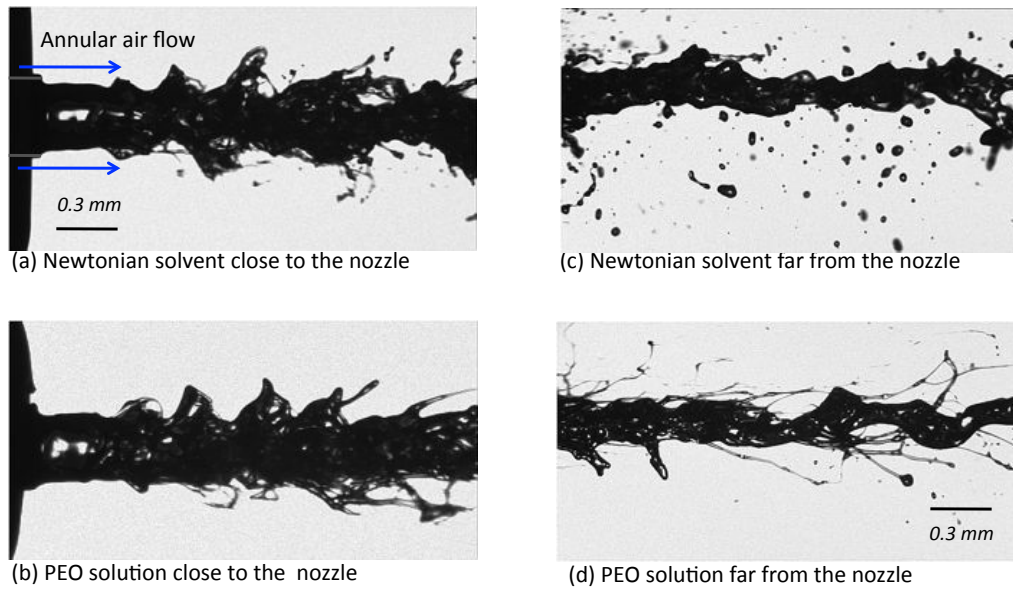
Figure 1: (a) Spray visualization images for the Newtonian solvent close to the nozzle. (b) Spray visualization images for the viscoelastic solution (PEO-300K-0.01 wt.% in the solvent) close to the nozzle. (c) Spray visualization images for the Newtonian solvent far from the nozzle. (d) Spray visualization images for the viscoelastic solution (PEO-300K-0.01 wt.% in the solvent) $5mm$ away from the nozzle.
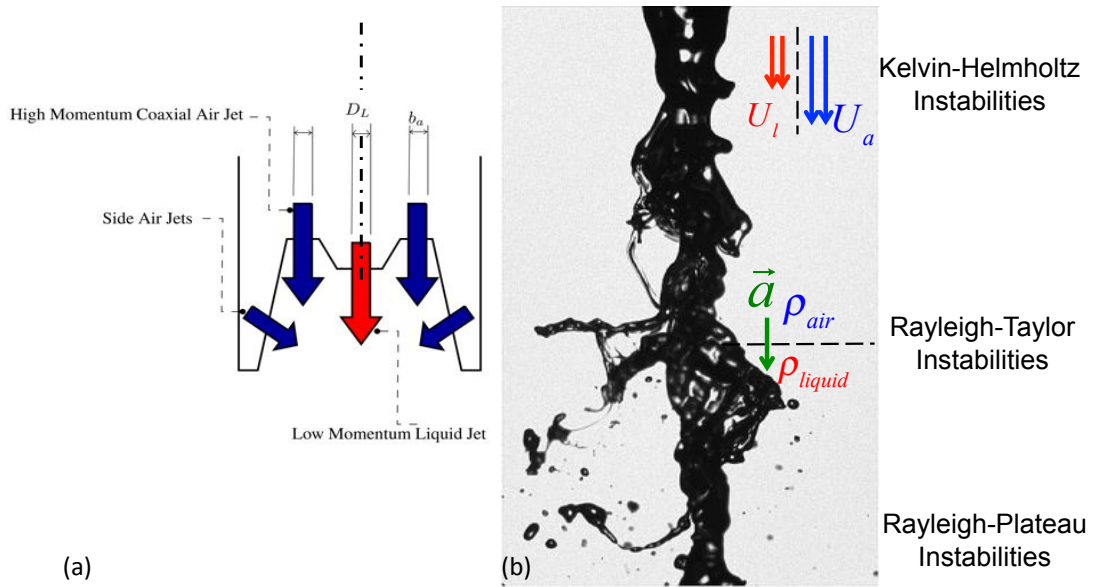
Figure 2: (a) Schematic of the industrial spray nozzle used in the experiments with $D_L = 1.5mm$, $b_a = 1.5mm$. A low momentum liquid jet (red color) is surrounded by a coaxial high momentum jet of air (blue color). The oblique air jets are low momentum and only help confine the primary jet in a narrow plane. (b) Spray visualization of water; three different successive instabilities make the liquid jet unstable and finally atomize it into a fine mist of droplets.
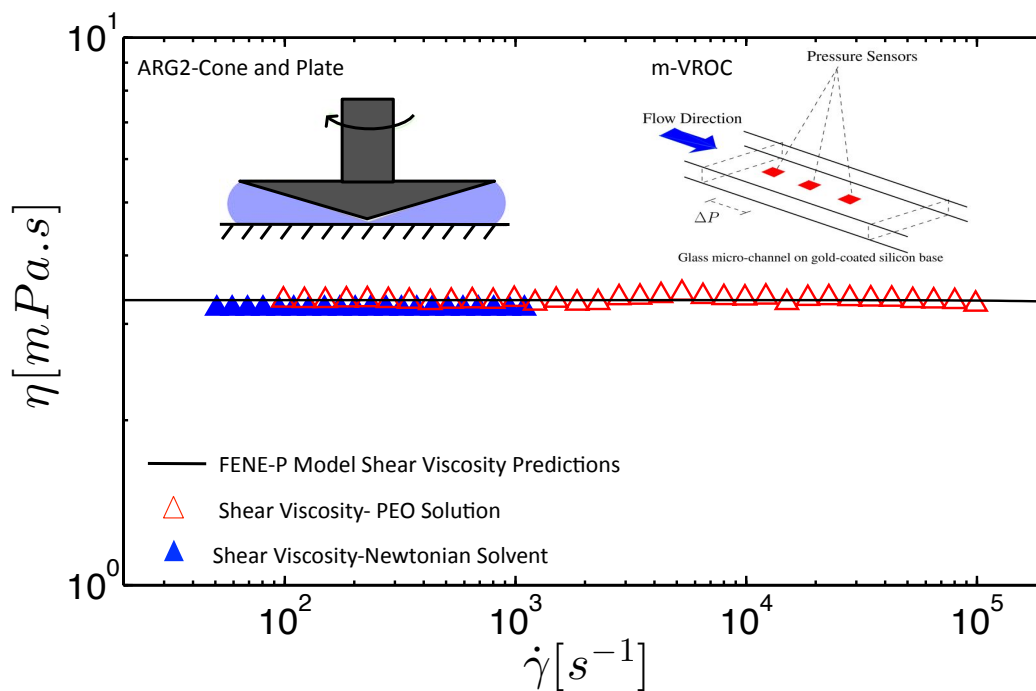
Figure 3: Shear rheology for both the Newtonian solvent and the dilute polymer solution (PEO-300K-0.01 wt.% in the solvent). The solid line shows the FENE-P prediction for steady shear using model parameters in table 1. The low shear rate measurements were done using a 40 mm cone and plate geometry in a torsional rheometer (AR-G2) and the high shear rate data are determined from pressure drop measurements in a micro-fluidic slit device (m-VROC).
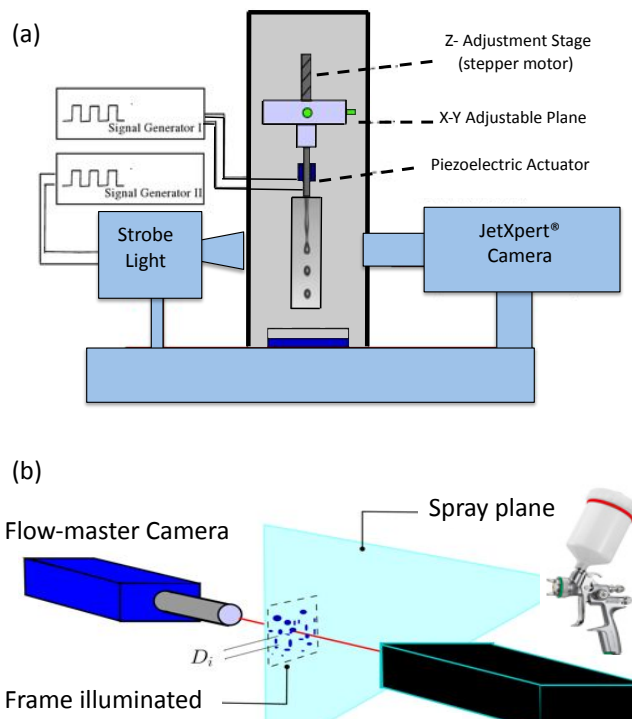
Figure 4: (a) The ROJER (Rayleigh-Ohnesorge Jetting Extensional Rheometer) setup. The liquid jet is perturbed by a piezo-electric actuator and then its motion is slowed down and captured using the stroboscope imaging setup. (b) The LaVision spray visualization setup. A 1.5mm × 1.5mm frame is illuminated using laser back-lighting and a Flowmaster camera captures individual snapshots from the droplets in the spray fan.
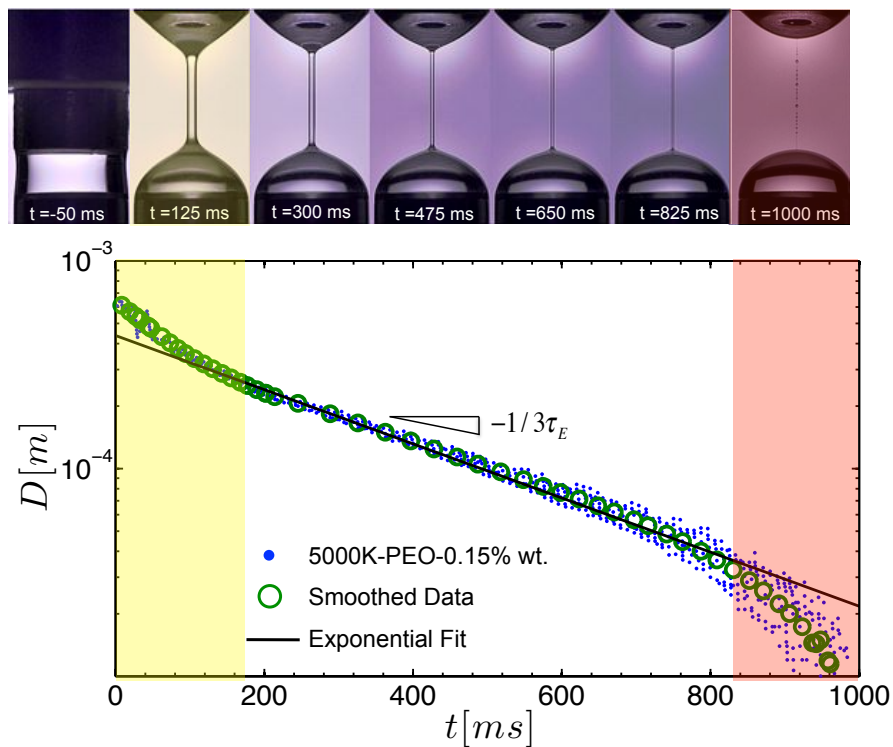
Figure 5: CaBER (Capillary Breakup Extensional Rheometry) for a semi-dilute Poly(ethylene oxide) solution (molecular weight $Mw = 5 \times 10^6 g/mol$ and 0.15 wt.% concentration,$c/c^* = 1.5$), $Oh = 0.005, De = 1.72$. The blue dots are the oversampled data from the laser micrometer while the green circles are the bin-averaged smoothed data. The visualized images of the actual filament thinning with time are at the top. The filament goes through three significant regimes: the initial region (shaded yellow) is still affected by fluid inertia; as the liquid thread thins down under the action of capillary pressure the elastic stresses become increasingly important and an elasto-capillary region emerges. The solid black line indicates an exponential decay with time described by Eq. (10) (the theoretical prediction for elasto-capillary regime). Finally when the polymer chains in the filament approach their maximum extensibility the diameter approaches zero in a linear manner (shaded orange region).
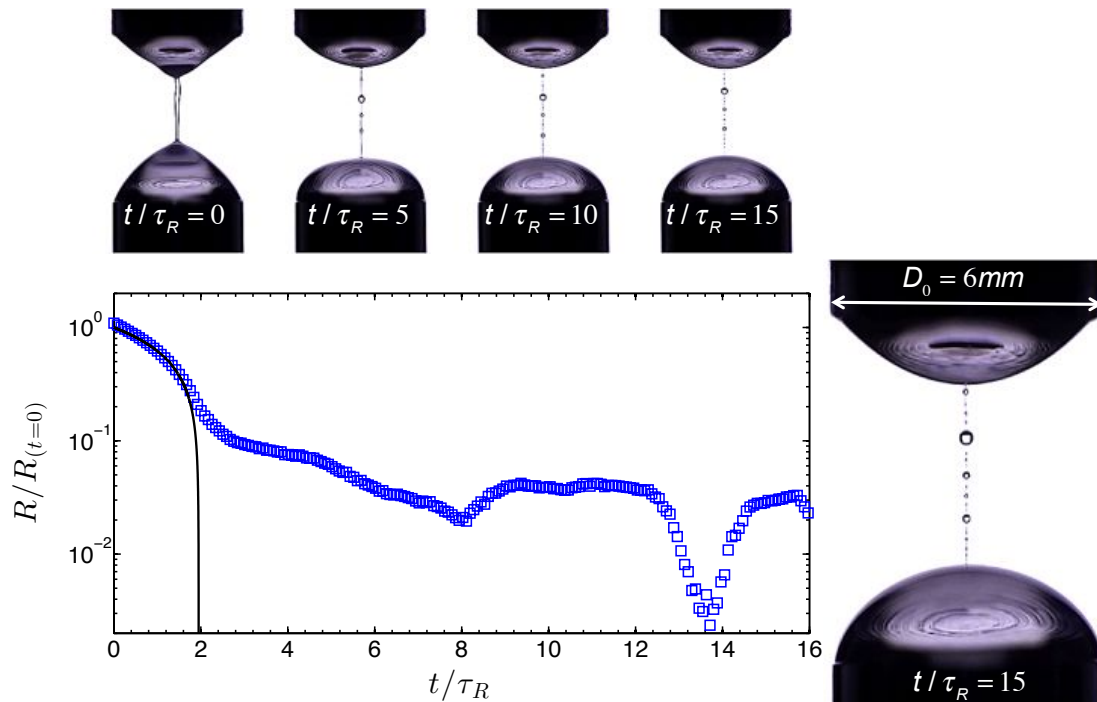
Figure 6: CaBER (Capillary Breakup Extensional Rheometry) for a dilute poly ethylene oxide solution ($M_w = 2 \times 10^6 g/mol$ and 0.01 wt.% concentration $c/c^* = 0.1$),$Oh = 0.01, De = 0.1$. The blue squares show the data from the laser micrometer; the normalized filament diameter is plotted versus time normalized by the capillary time-scale($\tau_R \equiv \sqrt{\rho R_{(t=0)}^3/\sigma} = 6ms$). The solid line is a fit from the expected predictions for inertia-capillary regime (Eq. (7) in the text). The visualized images of the actual filament thinning with time are shown above. The beads-on-a-string structure that appears in the final stages (picture on the right) makes the measurements of relaxation time almost impossible as the midplane diameter rises and falls with time.
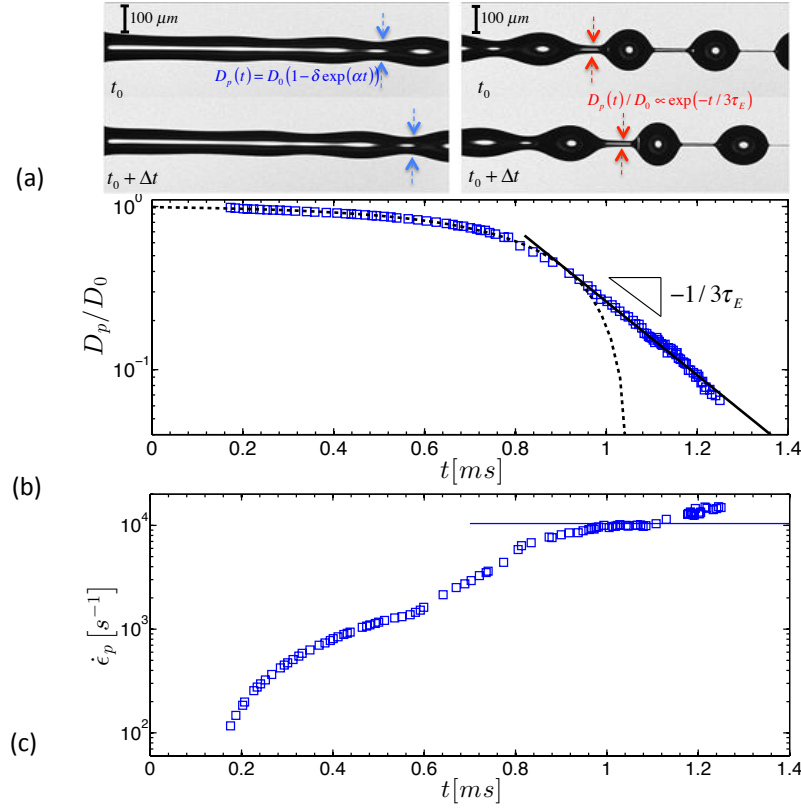
Figure 7: Rayleigh-Ohnesorge Jetting Extensional Rheometry (ROJER) analysis for the 300K-PEO solution ($c/c^* = 0.036$); $We_j = 16.9, kR_0 = 0.8, Oh = 0.075, De = 0.72$;(a) Visualized images of the jet going through Rayleigh-Plateau instability; both the linear stage of the instability (left) and the nonlinear stage (right) were imaged using the strobe camera. (b) The measured values for the filament diameter plotted against time (blue squares). The dashed line is the fit from the linear instability analysis ($D/D_0 = 1 - \delta \, exp(\alpha(We, Oh, De)t)$) with $\delta = 0.01$). The solid black line indicates exponential decay with time described by Eq. (10) as the theoretical prediction for elasto-capillary regime. From fitting the exponential region, the value of the relaxation time is found to be equal to $\tau_E = 60\mu s$. (c) Strain rate in the filament neck ($\dot{\epsilon} \equiv (-2/D(t)) \, dD(t)/dt$) versus time. The calculated values show a plateau at a critical stain rate equal to $2/3\tau_E$ (solid black line).
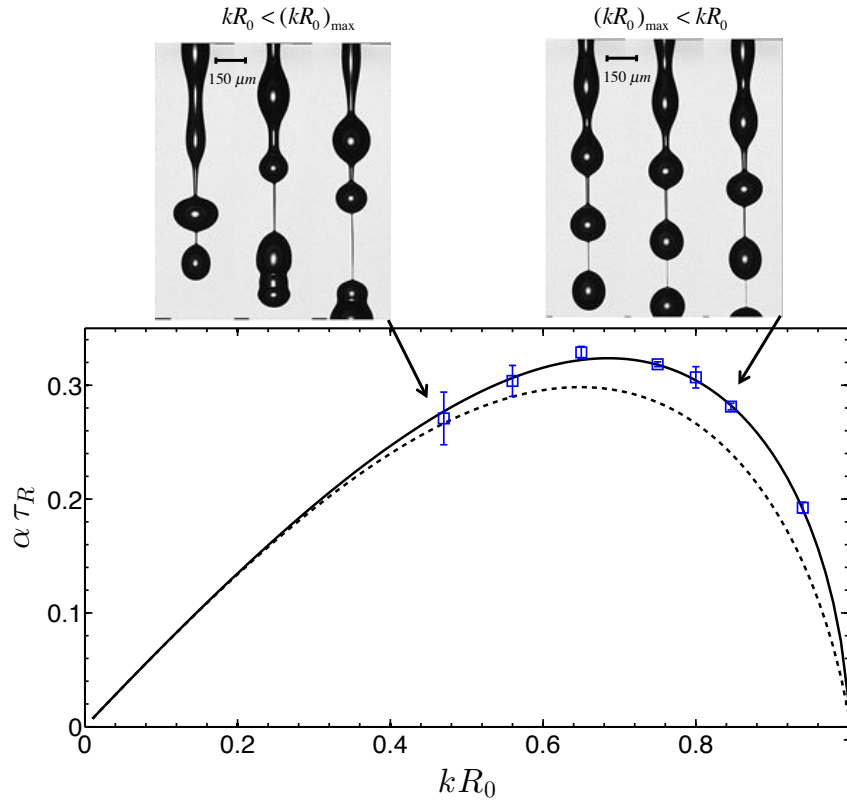
Figure 8: Values of dimensionless growth rate $(\alpha\tau_R)$ for the instability measured from experiments at different dimensionless wave-numbers (kR_0) for the viscoelastic jet (PEO 300K) with $Oh = 0.075, We = 16.9, De = 0.72$, (blue squares) compared with the theoretical dispersion curve for the Rayleigh-Plateau instability: the dashed line shows the dispersion curve for a Newtonian jet $(Oh = 0.075, We = 16.9)$ and the solid line is for the viscoelastic jet $(Oh = 0.075, We = 16.9, De = 0.72)$. Theoretical results are evaluated from the linear instability analysis of Brenn et al.[74]. Also shown is a montage of images from the final stages of breakup for two different wavenumbers: the left image for $kR_0 = 0.43$ is below the most unstable wavenumber $(kR_0 < (kR_0)_{max})$ and clearly shows the growth of higher wavenumber modes leading to the appearance of a large satellite droplet which later merges into the leading drop, the right image shows a wavenumber of $kR_0 = 0.80$ that is larger than the most unstable mode and for which the satellite droplets do not appear resulting in a smooth beads-on-a-string structure.
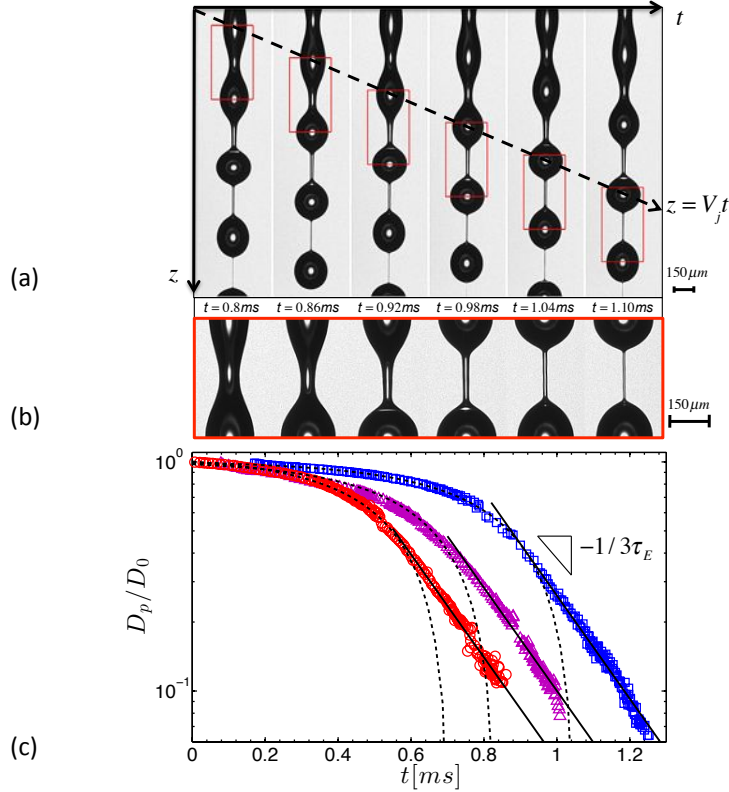
Figure 9: (a) Montage of images obtained at different times from the jet breakup experiment ($We_j = 16.9, kR_0 = 0.8, Oh = 0.075, De = 0.72$) following a fixed Lagrangian fluid element (i.e. the section of the jet shown in the red box) which moves with constant velocity ($V_j = 2.6ms^{-1}$).(b) Sitting in a moving frame translating with constant velocity (V_j) the Lagrangian element becomes stationary and the filament thins down as a results of capillarity in a way that is reminiscent of the dynamics of the filament in CaBER. (c) The normalized diameter versus time for PEO-300K-0.01 wt.%($Oh = 0.075, De = 0.7$) at three different jet velocities: red circles ($V_j = 3.9ms^{-1}, We = 39.6, kR_0 = 0.66$), magenta triangles ($V_j = 4.7ms^{-1}, We = 54.5, kR_0 = 0.80$), blue squares ($V_j = 2.6ms^{-1}, We = 16.9, kR_0 = 0.80$). The dashed lines are the corresponding fits from the linear instability analysis ($D/D_0 = 1 - \epsilon \, exp(\alpha(We, Oh, De)t)$) and the solid lines each show an exponential decay ($D/D_0 \sim exp(-t/3\tau_E)$) with $\tau_E = 60\mu s$ for each line. The measured relaxation times from ROJER analysis are thus independent of jet velocity.
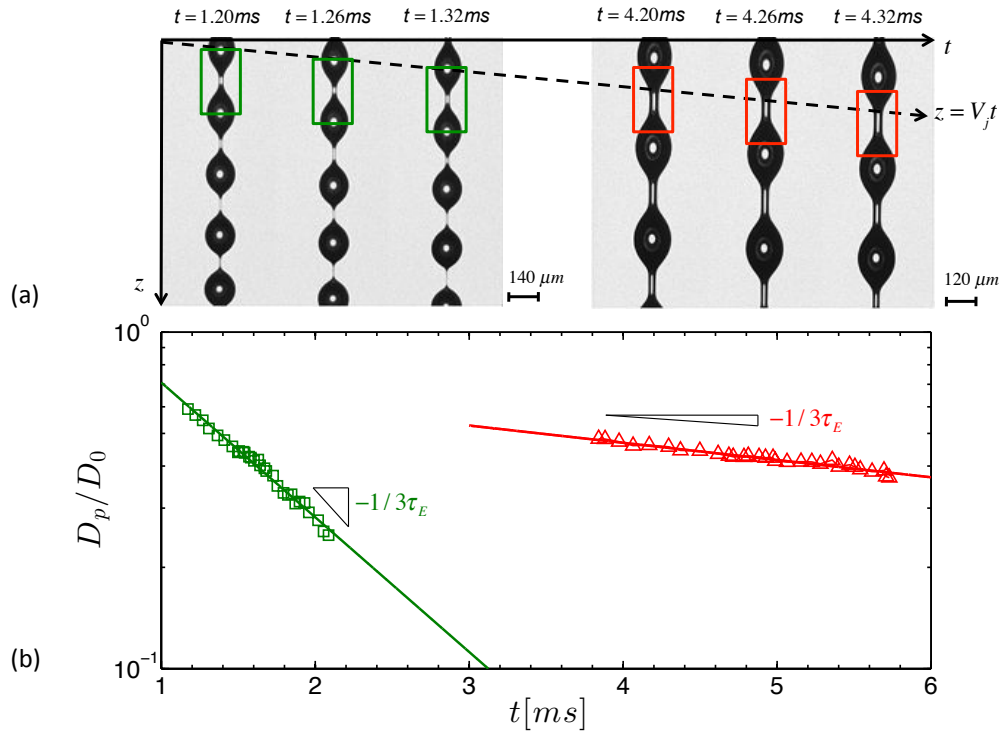
Figure 10: (a) Montage of images from ROJER test for two different molecular weight polymer solutions (left images are for PEO-300K-0.1 wt.% and the right images are for PEO-1000K-0.05 wt.% $We_j = 8.5, kR_0 = 0.77, Oh = 0.075$) at different times following a Lagrangian fluid element (the section of jet in the green and red boxes respectively) which moves with constant velocity ($V_j = 0.87ms^{-1}$).(b) The normalized diameter versus time for PEO-300K-0.1 wt.% (green squares) and for PEO-1000K-0.05 wt.% (red triangles). The solid lines show exponential decays fitted to Eq. (10) with $\tau_E = 360\mu s$ for PEO-300K-0.1 wt.% and $\tau_E = 2800\mu s$ for PEO-1000K-0.05wt.%.
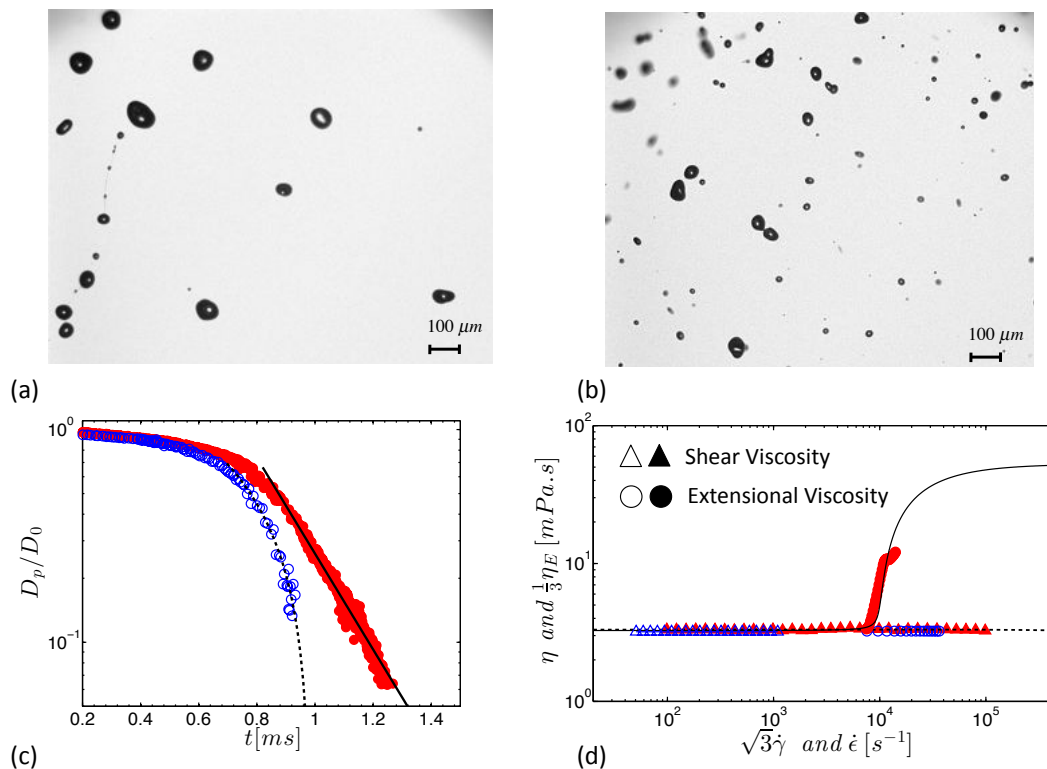
(a)

(b)

(c)

(d)

Figure 11: (a) Visualization of viscoelastic droplets (PEO-300K-0.01 wt.%) undergoing fragmentation in opposed jet atomization ($Re = 620, We = 300$). (b) Visualization of Newtonian solvent droplets (water and glycerol 60-40 wt.%,$Re = 620, We = 300$) during fragmentation in opposed jet atomization. (c) The ROJER measurements of the thinning filament diameter as a function of time for both the viscoelastic liquid (PEO-300K-0.01 wt.%-red filled circles) and the corresponding Newtonian solvent (water and glycerol ,60-40 wt.%-blue open circles). Solid line shows the exponential fit for the elasto-capillary regime (Eq. (10)) and the dashed line is the linear fit for the visco-capillary regime for filament thinning ($D(t) = 0.072 \, (\sigma/\eta_s) \, (t_b - t)$). (d) Shear (triangle) and extensional rheology (circle) for both the Newtonian solvent (blue open symbols) and the viscoelastic solution (PEO-300K-0.01 wt.%)(red filled symbols). The solid and dashed lines show respectively the FENE-P predictions using model parameters in Table 1 for the extensional and shear viscosities. The transient elongational viscosity data are extracted from the jet thinning dynamics shown in Figure 11(c).
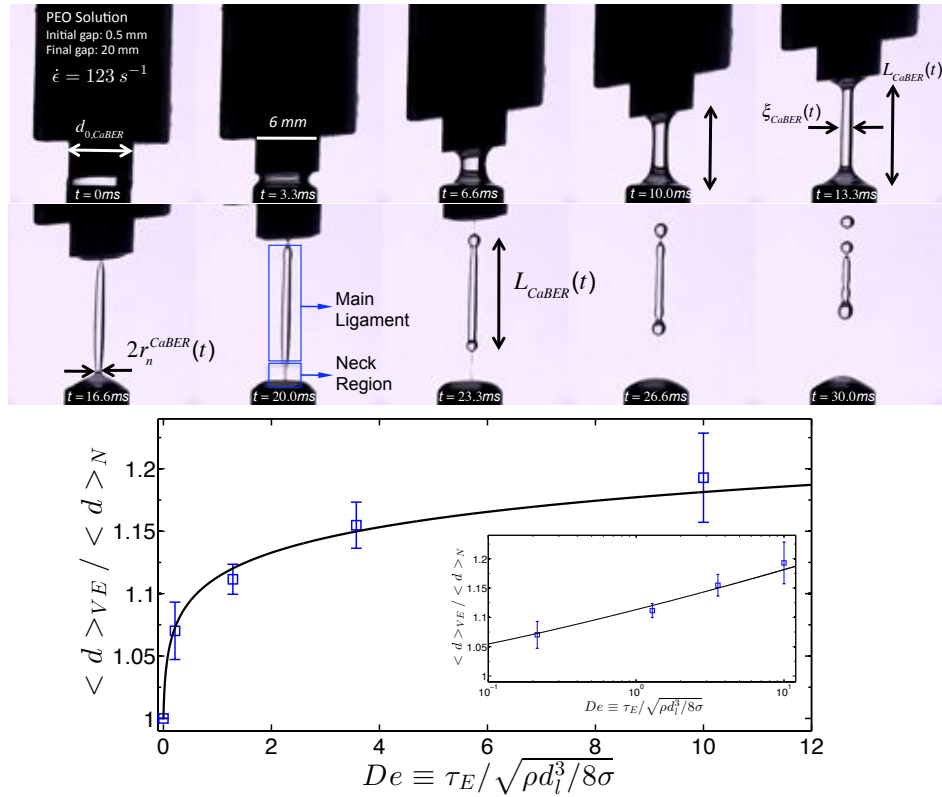
Figure 12: (a) Montage of images from the sudden stretch experiment for PEO-300K-0.01 wt.%. (b) Blue squares are average sizes for the viscoelastic solutions normalized by the average diameter for solvent drops as a function of the Deborah (De) number in the ligament ($De \equiv \tau_E/\sqrt{\rho d_0^3/8\sigma}$ in which d_0 is the characteristic ligament size and is estimated from the average diameter, $<d>$). The solid black line shows the predictions from the model described in the text (Eq. (19)).

References

[1] J. Eggers and E. Villermaux, "Physics of liquid jets," *Reports on Progress in Physics*, vol. 71, no. 3, 2008.

[2] A. H. Lefebvre, *Atomization and Sprays.* Hemisphere Publishing Corporation, 1989.

[3] P. Marmottant and E. Villermaux, "Fragmentation of stretched liquid ligaments," *Physics of Fluids*, vol. 16, no. 8, p. 2732, 2004.

[4] A. Mansour and N. Chigier, "Air-blast atomization of non-Newtonian liquids," *Journal of Non-Newtonian Fluid Mechanics*, vol. 58, pp. 161–194, July 1995.

[5] K. Walters, "Theoretical and Applied Rheology," in *Theoretical and Applied Rheology* (P. Moldenaers and R. Keunings, eds.), (Brussels), pp. 16–23, Elsevier, 1992.

[6] J. W. Hoyt, "Recent progress in polymer drag reduction," *Research and Development Report, Jan. - Apr. 1974 Naval Undersea Center, San Diego, CA.*, vol. -1, Oct. 1974.

[7] K. K. Chao, C. A. Child, E. A. Grens, and M. C. Williams, "Antimisting action of polymeric additives in jet fuels," *AIChE Journal*, vol. 30, pp. 111–120, Jan. 1984.

[8] J. W. Hoyt and J. J. Taylor, "Turbulence structure in a water jet discharging in air," *Physics of Fluids*, vol. 20, p. S253, Oct. 1977.

[9] J. W. Hoyt, "Drag reduction-jet breakup correlation with kerosene-based additives," *Journal of Rheology*, vol. 24, p. 685, Oct. 1980.

[10] M. S. Owens, M. Vinjamur, L. Scriven, and C. Macosko, "Misting of non-Newtonian liquids in forward roll coating," *Journal of Non-Newtonian Fluid Mechanics*, vol. 166, pp. 1123–1128, Oct. 2011.

[11] B. J. de Gans, P. C. Duineveld, and U. S. Schubert, "Inkjet printing of polymers: State of the art and future developments," *Advanced Materials*, vol. 16, no. 3, pp. 203–213, 2004.

[12] B. Derby, "Inkjet printing of functional and structural materials: fluid property requirements, feature stability, and rsesolution," in *Annual Review of Materials Research, Vol 40*, vol. 40, pp. 395–414, 2010.

[13] N. Arockiam, "The future of aerospace propulsion: viscoelastic non-Newtonian liquids," *Journal of Purdue Undergraduate Research*, vol. 1, pp. 2–9, Aug. 2011.

[14] J. A. Mallory, S. J. DeFini, and P. E. Sojka, "Formulation of gelled propellant simulants," in *46th AIAA/ASME/SAE/ASEE Joint Propulsion Conference & Exhibit*, 2010.

[15] J. E. Matta, R. P. Tytus, and J. L. Harris, "Aerodynamic atomization of polymeric solutions," *Chemical Engineering Communications*, vol. 19, pp. 191–204, Jan. 1983.

[16] R. B. Bird, R. C. Armstrong, and O. Hassager, *Dynamics of Polymeric Liquids*, vol. 1. New York: John Wiley & Sons, 2nd ed., 1987.

[17] J. C. Thompson and J. P. Rothstein, "The atomization of viscoelastic fluids in flat-fan and hollow-cone spray nozzles," *Journal of Non-Newtonian Fluid Mechanics*, vol. 147, no. 1-2, pp. 11–22, 2007.

[18] Y. Christanti and L. M. Walker, "Quantifying air atomization of viscoelastic fluids through fluid relaxation times," *Atomization and Sprays*, vol. 16, no. 7, pp. 777–790, 2006.

[19] C. J. S. Petrie, *Elongational Flows*. London: Pitman, 1979.

[20] D. F. James and K. Walters, "A Critical Appraisal of Available Methods for the Measurement of Extensional Properties of Mobile Systems," in *Techniques in Rheological Measurement SE - 2* (A. A. Collyer, ed.), pp. 33–53, Springer Netherlands, 1993.

[21] L. E. Rodd, T. P. Scott, J. J. Cooper-White, and G. H. McKinley, "Capillary break-up rheometry of low-viscosity elastic fluids," *Applied Rheology*, vol. 15, no. 1, pp. 12–27, 2005.

[22] C. J. S. Petrie, "Extensional viscosity: A critical discussion," *Journal of Non-Newtonian Fluid Mechanics*, vol. 137, no. 1-3, pp. 15–23, 2006.

[23] C. J. S. Petrie, "One hundred years of extensional flow," *Journal of Non-Newtonian Fluid Mechanics*, vol. 137, no. 1-3, pp. 1–14, 2006.

[24] C. Clasen, P. M. Phillips, L. Palangetic, Vermant, and Jan, "Dispensing of rheologically complex fluids: The map of misery," *AIChE Journal*, vol. 58, pp. 3242–3255, Oct. 2012.

[25] G. H. McKinley and T. Sridhar, "Filament-stretching rheometry of complex fluids," *Annual Review of Fluid Mechanics*, vol. 34, pp. 375–415, 2002.

[26] D. Binding and K. Walters, "On the use of flow through a contraction in estimating the extensional viscosity of mobile polymer solutions," *Journal of Non-Newtonian Fluid Mechanics*, vol. 30, pp. 233–250, Jan. 1988.

[27] B. Yesilata, C. Clasen, and G. H. McKinley, "Nonlinear shear and extensional flow dynamics of wormlike surfactant solutions," *Journal of Non-Newtonian Fluid Mechanics*, vol. 133, no. 2-3, pp. 73–90, 2006.

[28] T. R. Tuladhar and M. R. Mackley, "Filament stretching rheometry and break-up behaviour of low viscosity polymer solutions and inkjet fluids," *Journal of Non-Newtonian Fluid Mechanics*, vol. 148, no. 1-3, pp. 97–108, 2008.

[29] D. C. Vadillo, "Evaluation of the inkjet fluid's performance using the "Cambridge Trimaster" filament stretch and break-up device," *Journal of rheology*, vol. 54, no. 2, pp. 261 – 282, 2010.

[30] L. Campo-Deaño and C. Clasen, "The slow retraction method (SRM) for the determination of ultra-short relaxation times in capillary breakup extensional rheometry experiments," *Journal of Non-Newtonian Fluid Mechanics*, vol. 165, pp. 1688–1699, Dec. 2010.

[31] D. C. Vadillo, W. Mathues, and C. Clasen, "Microsecond relaxation processes in shear and extensional flows of weakly elastic polymer solutions," *Rheologica Acta*, vol. 51, pp. 755–769, July 2012.

[32] S. Chandrasekhar, *Hydrodynamic and Hydromagnetic Stability*. Dover Publications, 1961.

[33] Y. Christanti and L. M. Walker, "Surface tension driven jet break up of strain-hardening polymer solutions," *Journal of Non-Newtonian Fluid Mechanics*, vol. 100, no. 1-3, pp. 9–26, 2001.

[34] P. Schümmer and K. H. Tebel, "Design and operation of the free jet elongational rheometer," *Rheologica Acta*, vol. 21, no. 4-5, pp. 514–516, 1982.

[35] J. Ferguson, N. Hudson, and B. Warren, "The break-up of fluids in an extensional flow field," *Journal of Non-Newtonian Fluid Mechanics*, vol. 44, pp. 37–54, Sept. 1992.

[36] L. E. Rodd, T. P. Scott, D. V. Boger, J. J. Cooper-White, and G. H. McKinley, "The inertio-elastic planar entry flow of low-viscosity elastic fluids in micro-fabricated geometries," *Journal of Non-Newtonian Fluid Mechanics*, vol. 129, no. 1, pp. 1–22, 2005.

[37] S. J. Haward, M. S. N. Oliveira, M. A. Alves, and G. H. McKinley, "Optimized cross-slot flow geometry for microfluidic extensional rheometry," *Physical Review Letters*, vol. 109, p. 128301, Sept. 2012.

[38] D. F. James, "Boger fluids," *Annual Review of Fluid Mechanics*, vol. 41, pp. 129–142, 2009.

[39] P. Schümmer and K. H. Tebel, "A new elongational rheometer for polymer solutions," *Journal of Non-Newtonian Fluid Mechanics*, vol. 12, no. 3, pp. 331–347, 1983.

[40] H. E. Edgerton, *Electronic Flash, Strobe.* Massachussetts Institute of Technology(MIT), 1987.

[41] S. P. Lin, *Breakup of Liquid Sheets and Jets.* Cambridge University Press, 2010.

[42] F. T. Trouton, "On the coefficient of viscous traction and its relation to that of viscosity," *Proceedings of the Royal Society of London. Series A*, vol. 77, pp. 426–440, May 1906.

[43] S. L. Anna, G. H. McKinley, D. A. Nguyen, T. Sridhar, S. J. Muller, J. Huang, and D. F. James, "An interlaboratory comparison of measurements from filament-stretching rheometers using common test fluids," *Journal of Rheology*, vol. 45, p. 83, Jan. 2001.

[44] M. L. Sentmanat, "Miniature universal testing platform: from extensional melt rheology to solid-state deformation behavior," *Rheologica Acta*, vol. 43, pp. 657–669, Aug. 2004.

[45] M. L. Sentmanat, B. N. Wang, and G. H. McKinley, "Measuring the transient extensional rheology of polyethylene melts using the SER universal testing platform," *Journal of Rheology*, vol. 49, no. 3, pp. 585–606, 2005.

[46] A. V. Bazilevsky, V. M. Entov, and A. N. Rozhkov, "Liquid Filament Microrheometer and Some of Its Applications," in *Third European Rheology Conference and Golden Jubilee Meeting of the British Society of Rheology SE - 21* (D. R. Oliver, ed.), pp. 41–43, Springer Netherlands, 1990.

[47] G. H. McKinley, "Visco-elasto-capillary thinning and breakup of complex fluids," *Rheology Reviews*, pp. 1–48, 2005.

[48] G. H. McKinley and A. Tripathi, "How to extract the Newtonian viscosity from capillary breakup measurements in a filament rheometer," *Journal of Rheology*, vol. 44, no. 3, pp. 653–670, 2000.

[49] R. Sattler, S. Gier, J. Eggers, and C. Wagner, "The final stages of capillary break-up of polymer solutions," *Physics of Fluids*, vol. 24, no. 2, p. 023101, 2012.

[50] V. M. Entov and E. J. Hinch, "Effect of a spectrum of relaxation times on the capillary thinning of a filament of elastic liquid," *Journal of Non-Newtonian Fluid Mechanics*, vol. 72, pp. 31–54, 1997.

[51] P. Erni, M. Varagnat, C. Clasen, J. Crest, and G. H. McKinley, "Microrheometry of sub-nanolitre biopolymer samples: non-Newtonian flow phenomena of carnivorous plant mucilage," *Soft Matter*, vol. 7, p. 10889, Nov. 2011.

[52] C. Clasen, J. P. Plog, W. M. Kulicke, M. Owens, C. Macosko, L. E. Scriven, M. Verani, and G. H. McKinley, "How dilute are dilute solutions in extensional flows?," *Journal of Rheology*, vol. 50, no. 6, pp. 849–881, 2006.

[53] O. Arnolds, H. Buggisch, D. Sachsenheimer, and N. Willenbacher, "Capillary breakup extensional rheometry (CaBER) on semi-dilute and concentrated polyethyleneoxide (PEO) solutions," *Rheologica Acta*, vol. 49, pp. 1207–1217, Nov. 2010.

[54] P. P. Bhat, S. Appathurai, M. T. Harris, M. Pasquali, G. H. McKinley, and O. A. Basaran, "Formation of beads-on-a-string structures during break-up of viscoelastic filaments," *Nature Physics*, vol. 6, pp. 625–631, June 2010.

[55] M. S. N. Oliveira and G. H. McKinley, "Iterated stretching and multiple beads-on-a-string phenomena in dilute solutions of highly extensible flexible polymers," *Physics of Fluids*, vol. 17, no. 7, 2005.

[56] F. Savart, "Mémoire sur le choc dune veine liquide lancée contre un plan circulaire," *Ann. chim*, vol. 54, no. 56, p. 1833, 1833.

[57] J. Plateau, "Ueber die Gränze der Stabilität eines flüssigen Cylinders," *Annalen der Physik und Chemie*, vol. 156, no. 8, pp. 566–569, 1850.

[58] L. Rayleigh, "On the instability of jets," *Proceedings of the London Mathematical Society*, vol. 10, no. 1, pp. 4–13, 1878.

[59] J. Eggers, "Nonlinear dynamics and breakup of free-surface flows," *Reviews of Modern Physics*, vol. 69, no. 3, pp. 865–929, 1997.

[60] L. Rayleigh, "Some applications of photography," *Nature*, vol. 44, no. 249, p. 441, 1891.

[61] H. E. Edgerton, E. A. Hauser, and W. B. Tucker, "Studies in drop formation as revealed by the high-speed motion camera," *The Journal of Physical Chemistry*, vol. 41, pp. 1017–1028, July 1937.

[62] E. A. Hauser, H. E. Edgerton, B. M. Holt, and J. T. Cox, "The application of the high-speed motion picture camera to research on the surface tension of liquids.," *The Journal of Physical Chemistry*, vol. 40, pp. 973–988, Jan. 1935.

[63] R. Eötvös, "Ueber den Zusammenhang der Oberflächenspannung der Flüssigkeiten mit ihrem Molecularvolumen," *Annalen der Physik*, vol. 263, no. 3, pp. 448–459, 1886.

[64] N. Bohr, "Determination of the surface-tension of water by the method of jet vibration," *Philosophical Transactions of the Royal Society of London. Series A, Containing Papers of a Mathematical or Physical Character*, pp. 281–317, 1909.

[65] F. W. Kroesser and S. Middleman, "Viscoelastic jet stability," *AIChE Journal*, vol. 15, no. 3, pp. 383–&, 1969.

[66] S. Middleman, "Stability of a viscoelastic jet," *Chemical Engineering Science*, vol. 20, no. 12, pp. 1037–&, 1965.

[67] S. Middleman, *Modeling axisymmetric flows: Dynamics of films, jets and drops*. San Diego: Academic Press, 1995.

[68] D. W. Bousfield, R. Keunings, G. Marrucci, and M. M. Denn, "Nonlinear analysis of the surface tension driven breakup of viscoelastic filaments," *Journal of Non-Newtonian Fluid Mechanics*, vol. 21, no. 1, pp. 79–97, 1986.

[69] P. Schümmer and K. H. Tebel, "The use of controlled jet instability for elongational rheometry," *Journal of Rheology*, vol. 26, no. 1, pp. 77–78, 1982.

[70] A. V. Bazilevsky, V. M. Entov, A. N. Rozhkov, and A. L. Yarin, "Polymeric Jets Beads-on-String Breakup and Related Phenomena," in *Third European Rheology Conference and Golden Jubilee Meeting of the British Society of Rheology SE - 22* (D. R. Oliver, ed.), pp. 44–46, Springer Netherlands, 1990.

[71] V. M. Entov and A. L. Yarin, "Influence of elastic stresses on the capillary breakup of jets of dilute polymer solutions," *Fluid Dynamics*, vol. 19, no. 1, pp. 21–29, 1984.

[72] Y. Christanti and L. M. Walker, "Effect of fluid relaxation time of dilute polymer solutions on jet breakup due to a forced disturbance," *Journal of Rheology*, vol. 46, no. 3, pp. 733–748, 2002.

[73] V. Sharma, A. M. Ardekani, and G. H. McKinley, "Beads on a StringStructures and Extensional Rheometry using Jet Break-up," in *5th Pacific Rim Conference on Rheology (PRCR-5)*, 2010.

[74] G. Brenn, Z. B. Liu, and F. Durst, "Linear analysis of the temporal instability of axisymmetrical non-Newtonian liquid jets," *International Journal of Multiphase Flow*, vol. 26, no. 10, pp. 1621–1644, 2000.

[75] M. Goldin, J. Yerushalmi, R. Pfeffer, and R. Shinnar, "Breakup of a laminar capillary jet of a viscoelastic fluid," *Journal of Fluid Mechanics*, vol. 38, no. 04, pp. 689–711, 1969.

[76] A. M. Ardekani, V. Sharma, and G. H. McKinley, "Dynamics of bead formation, filament thinning and breakup in weakly viscoelastic jets," *Journal of Fluid Mechanics*, vol. 665, pp. 46–56, Dec. 2010.

[77] N. N. Mansour and T. S. Lundgren, "Satellite formation in capillary jet breakup," *Physics of Fluids A: Fluid Dynamics*, vol. 2, p. 1141, July 1990.

[78] R. P. Mun, J. A. Byars, and D. V. Boger, "The effects of polymer concentration and molecular weight on the breakup of laminar capillary jets," *Journal of Non-Newtonian Fluid Mechanics*, vol. 74, no. 1-3, pp. 285–297, 1998.

[79] L. Rayleigh, "On the capillary phenomenon of jets," *Proceedings of the Royal Society of London*, vol. 29, pp. 71–97, 1879.

[80] C. Clasen, J. Bico, V. M. Entov, and G. H. McKinley, "'Gobbling drops': the jetting-dripping transition in flows of polymer solutions," *Journal of Fluid Mechanics*, vol. 636, pp. 5–40, 2009.

[81] S. P. Lin and R. D. Reitz, "DROP and spray formation from a liquid jet," *Annual Review of Fluid Mechanics*, vol. 30, pp. 85–105, Jan. 1998.

[82] M. Doi and S. F. Edwards, *The Theory of Polymer Dynamics*. New York: Oxford University Press, 1988.

[83] V. Tirtaatmadja, G. H. McKinley, and J. J. Cooper-White, "Drop formation and breakup of low viscosity elastic fluids: Effects of molecular weight and concentration," *Physics of Fluids*, vol. 18, no. 4, 2006.

[84] R. B. Bird, C. F. Curtiss, R. C. Armstrong, and O. Hassager, *Dynamics of Polymeric Liquids, Kinetic Theory (Dynamics of Polymer Liquids Vol. 2) (Volume 2)*. Wiley-Interscience, 1987.

[85] A. Peterlin, "Hydrodynamics of macromolecules in a velocity field with longitudinal gradient," *Journal of Polymer Science Part B: Polymer Letters*, vol. 4, pp. 287–291, Apr. 1966.

[86] J. E. Matta and R. P. Tytus, "Viscoelastic breakup in a high velocity airstream," *Journal of Applied Polymer Science*, vol. 27, pp. 397–405, Feb. 1982.

[87] J. E. Matta, "Nonlinear viscoelastic breakup in a high-velocity airstream," *Technical Report, May 1979 - Apr. 1980 Army Armament Research and Development Command, Aberdeen Proving Ground, MD. Chemical Systems Lab.*, vol. -1, Mar. 1981.

[88] S. C. Geckler and P. E. Sojka, "Effervescent atomization of viscoelastic liquids : experiment and modeling," *Journal of Fluids Engineering*, vol. 130, no. 6, pp. 1–11, 2008.

[89] A. Aliseda, E. Hopfinger, J. Lasheras, D. Kremer, A. Berchielli, and E. Connolly, "Atomization of viscous and non-newtonian liquids by a coaxial, high-speed gas jet. Experiments and droplet size modeling," *International Journal of Multiphase Flow*, vol. 34, pp. 161–175, Feb. 2008.

[90] E. Villermaux, "The formation of filamentary structures from molten silicates: Peles hair, angel hair, and blown clinker," *Comptes Rendus Mécanique*, vol. 340, pp. 555–564, Aug. 2012.

[91] P. Marmottant and E. Villermaux, "On spray formation," *Journal of Fluid Mechanics*, vol. 498, pp. 73–111, Jan. 2004.

[92] D. T. Papageorgiou, "On the breakup of viscous liquid threads," *Physics of Fluids*, vol. 7, pp. 1529–1544, 1995.

[93] J. Eggers, "Universal pinching of 3D axisymmetric free-surface flow," *Physical Review Letters*, vol. 71, pp. 3458–3460, Nov. 1993.

[94] M. P. Brenner, J. R. Lister, and H. A. Stone, "Pinching threads, singularities and the number 0.0304...," *Physics of Fluids*, vol. 8, p. 2827, Nov. 1996.

Supplementary Material